5-2021

System for HIV-1 Treatment to the Brain

Caroline Rose Garcia
The University of Texas Rio Grande Valley

THE DEVELOPMENT OF A TENOFOVIR-LOADED NANODISC AND LIPOSOME BASED DELIVERY SYSTEM FOR HIV-1 TREATMENT TO THE BRAIN

A Thesis

by

CAROLINE ROSE GARCIA

Submitted to the Graduate College of
The University of Texas Rio Grande Valley
In partial fulfillment of the requirements for the degree of

MASTERS OF SCIENCE

May 2021

Major Subject: Biochemistry and Molecular Biology

THE DEVELOPMENT OF A TENOFOVIR LOADED NANODISC AND LIPOSOME BASED DELIVERY SYSTEM FOR HIV-1 TREATMENT TO THE BRAIN

A Thesis
by
CAROLINE ROSE GARCIA

COMMITTEE MEMBERS

Dr. Upal Roy, Ph.D
Chair of Committee

Dr. Sue Anne Chew, Ph.D
Committee Member

Dr. Alejandro Lopez-Juarez, Ph.D
Committee Member

May 2021

ABSTRACT

Garcia, Caroline Rose, The Development of a Tenofovir Loaded Nanodisc and Liposome Based Delivery System for HIV-1 Treatment to the Brain. Master of Science (MS), May 2021, 70 pp., 5 tables, 15 figures, references, 93 titles.

While HIV-1 treatment has been revolutionized by combination antiretroviral therapy in the past two decades, HIV-1 remains persistent in organs that don't allow easy penetration of anti-HIV drugs (e.g., brain) and cause persistent HIV-1 infections and inflammation. Researchers have turned towards nanotechnology-based drug carriers to combat this challenge, such as nanodiscoidal bicelles (ND) and liposomes. Bicelles entrap the drug in their interior hydrophobic core until metabolized by the body, and the payload can be released at the desired location in a controlled, long-lasting dosage. This study investigated the toxicity and extended-release of an anti-HIV drug-loaded within ND and liposomes for HIV-1 treatment to the brain. Results from both *in-vitro* and *in-vivo* characterization studies demonstrated that further optimization of the ND formulation needs to be adjusted towards liposomal structures for future studies.

DEDICATION

Completing my master studies would not have been possible without the love and never-ending support of my family and friends. My mother, Carolina L. Garcia, and my father, Raul M. Garcia, wholeheartedly motivated and encouraged me into accomplishing this degree. Their ceiling has been my floor, and I could not thank them enough for their love and support. *Por ustedes and para ustedes*. Thank you to my brother, Nicholas Garcia, who has always been proud of me and encouraged me to do better.

I would also like to dedicate this thesis to my closest cousins, Marissa Garcia and Samantha Buentello, for being by my side every step of the way and for always listening to me when I needed it most. This thesis is also dedicated to Cooper G.; I couldn't have done this without your constant companionship.

ACKNOWLEDGEMENTS

I am grateful to Dr. Upal Roy, the chair of my dissertation committee, for his guidance and advice. From accepting me into his research lab to helping me with research design, thought processing, and manuscript editing, he has encouraged me and has been diligent in our work every step of the way. Thank you for your patience and understanding. Thank you to my thesis committee members: Dr. Sue Anne Chew and Dr. Alejandro Lopez-Juarez. Their advice, input, and comments on my dissertation helped ensure my research and work quality to be the best possible. Thank you to our collaborators at the University of Connecticut: Farnoosh Saeedinejad, Dr. Armin Tahmasbi Rad, and Dr. Mu-Ping Nieh. I would also like to thank my program coordinator, Dr. Michael Persans, for his guidance throughout this program. Thank you to Mrs. Deepa Roy for her assistance and support. I would like to acknowledge my fellow research lab members for their assistance and cooperation. Thank you to my KDChi sisters for your continuous motivation these past two years. Additional thanks goes to SRI Biosciences and UT Southwestern Medical Center for their assistance throughout this project.

This project has been funded in part with federal funds from the National Institute of Allergy and Infectious Diseases, National Institutes of Health, Department of Health and Human Services, under Contract No. HHSN272201400006I and partial NIH Grants #1R15NS108815-01 and #1R01AI147731-01A1. Additionally, internal funding has been provided by the University of Texas Rio Grande Valley.

TABLE OF CONTENTS

Page

LIST OF TABLES

Page

LIST OF FIGURES

Page

LIST OF ABBREVIATIONS

Abbreviation	Explanation
AIDS	Acquired Immunodeficiency Syndrome
ART	Antiretroviral therapy
BBB	Blood-brain barrier
cART	Combination antiretroviral therapy
CNS	Central nervous system
HAND	HIV-1 associated neurological disorders
HMC-3	Human microglial clone 3 cell line
HIV-1	Human immunodeficiency virus 1
MTD	Maximum tolerated dose
MTS	3-(4,5-dimethylthiazol-2-yl)-5-(3-carboxymethoxyphenyl)-2-(4-sulfophenyl)-2H-tetrazolium); cell viability assay
NP	Nanoparticle
ND	Nanodisc
PK	Pharmacokinetics
ROS	Reactive oxygen species
SH-SY5Y	Neuroblastoma cell line
TFV	Tenofovir

CHAPTER I

INTRODUCTION

HIV-1 and its Conventional Antiretroviral Therapy

First identified in 1981, the Human Immunodeficiency Virus (HIV-1) is a deadly retrovirus that, as of 2019, affects 38 million people worldwide [1]. Since the start of the HIV-1 global epidemic, 75.7 million people have become infected with HIV, and the virus has claimed the lives of 32.7 million people through AIDS-related illnesses [1]. After almost 40 years since its discovery, there is still no effective cure or preventative vaccine for HIV-1.

HIV-1 weakens the immune system by infecting and destroying CD4+ T-cells, white blood cells with the primary CD4+ receptor for infection [2]. HIV-1 attaches to the CD4+ protein on the surface of T cells and other cells to gain entry for infection. Additional chemokine receptor (CCR5 and CXCR4) have also been attributed as a “second doorway” that play a major role for HIV-1 to infect cells such as monocytes and dendritic cells [2]. HIV-1 can induce cell death in both uninfected and infected T cells [3]. The virus is most commonly spread by contact with bodily fluids of a person with HIV-1 infection, specifically through unprotected sex or sharing of drug injection equipment. When left untreated or detected too late, HIV-1 can destroy CD4+ T-cells, reducing the body's ability to fight off the infections and ultimately, lead to acquired immunodeficiency syndrome (AIDS). A CD4+ count is often used to check HIV-1

infected patients' health since HIV-1 causes severe damage to the immune system by targeting CD4+ cells. If a person's CD4+ cell count falls below 200 cell/mm^3, they become at risk of contracting an opportunistic infection [4].

HIV-1 treatment has been revolutionized by significant progress in effective prevention, diagnosis, and therapeutic options available [5]. Once a fatal disease, HIV-1 infection has been transformed into a manageable chronic illness enabling patients to live long and healthy lives with appropriate measures [5]. HIV treatment involves antiretroviral therapy (ART) that works to control HIV-1 within the body that is most effective by taking a combination of multiple drugs, which is known as combination antiretroviral therapy (cART) [5]. While cART helps reduce morbidity caused by HIV-1, it does not cure the HIV-1 infection; it suppresses viral replication within a person's body and allows an individual immune system to strengthen and regain its capability to fight off infections. People living with HIV are recommended to take their cART drugs every day of their lives to reduce the amount of HIV in the body to a deficient level [6]. When patients do not accurately adhere to their treatment regimen schedule and take their drugs too late, too early or entirely miss doses completely, their blood concentrations can drop below the necessary level in order to fully suppress HIV which can result in drug resistance that can severely limit future treatment options [6]. Drug resistance mutations proliferate during nonsuppressive antiretroviral therapy, typically the result of inadequate drug exposure which can severely limit future treatment options [6, 7]. There is still continuous research to try to improve the therapeutic options available, to control viral replication with minimal side effects successfully, and to be able to provide a manageable therapeutic regimen.

The Treatment Revolution

The first significant step in the treatment revolution of HIV-1 occurred when the virus's life cycle was characterized, and the medical and scientific community began to investigate antiretroviral approaches [5]. Researchers made progress towards HIV-1 therapy in 1987, where the antiretroviral drug, azidothymidine, was found to decrease mortality and opportunistic infection in AIDS patients [5]. Azidothymidine belongs to a class of drugs known as nucleoside transcriptase inhibitors (NRTIs), which block the reverse transcription step of the HIV-1 life cycle by disrupting the copying process through blockage of the reverse enzyme transcriptase [5]. However, viral resistance to the drug quickly developed, pushing the need for new drugs to be produced based on the HIV-1 replication cycle and how to target it [5]. Viral resistance led to introducing a therapeutic regimen that included a protease inhibitor (PI) alongside two nucleoside reverse transcriptase inhibitors (NRTIs) in cART to reduce morbidity and mortality [5].

Today, a person’s initial HIV-1 regimen will typically include three medicines from at least two different HIV drug classes to help effectively reduce viral load within a patient’s body. As of 2020, there are currently six major drug classes of antiretroviral drugs: entry inhibitors, fusion inhibitors, NRTIs, non-nucleoside reverse transcriptase inhibitors (NNRTIs), integrase inhibitors, and PIs [8]. Each of these drug classes works by interrupting various steps throughout the HIV-1's life cycle.

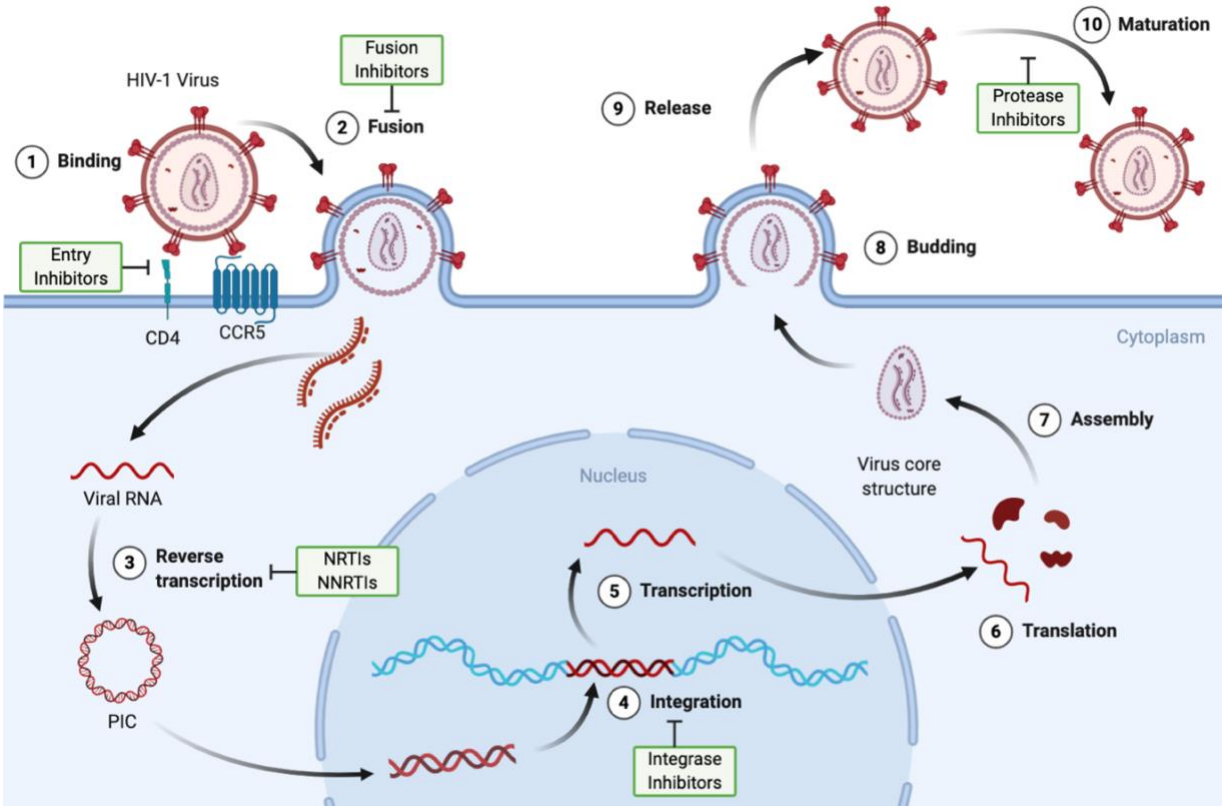

Figure 1: Schematic overview of the HIV-1 replication cycle*; figure illustrates ten main steps throughout the HIV-1 replication cycle where six major classes of antiretroviral drugs block a step in the life cycle. Entry inhibitors prevent HIV-1 from entering CD4 host cells at step 1 and fusion inhibitors prevent the HIV-1 from fusing with the host cell's membrane at step 2. NRTIs NNRTIs interfere with the HIV-1 reverse transcriptase enzyme at step 3. Integrase inhibitors block HIV-1 DNA from integrating with the host cell's genome at step 4. PIs block the protease enzyme's action and prevent the virus from multiplying at step 10. Figure adapted from BioRender.com.*

The HIV-1 replication cycle (Figure 1) begins with the virus entering cells by membrane fusion mediated by its envelope (*Env)* glycoproteins, gp120, and gp41. The gp120 first binds to the CD4+ receptor and co-receptor (CCR5) on the cell membrane [5, 9]. The gp41 then interacts with the target cell membrane through the N-terminal fusion domain to promote lipid mixing

and, ultimately, viral entry [9]. Entry inhibitors work to bind to the proteins on HIV-1, preventing it from attaching itself to and entering a CD4+ cell [8]. The virus binding to the CD4+ receptors and co-receptors allows for the fusion with the host cell membrane. This is where fusion inhibitors act and block the HIV envelope from fusing with the CD4+ membrane. If the virus continues to fuse, the viral capsid will be uncoated, and the HIV-1 RNA and proteins are released into the cytoplasm. The RNA and proteins then begin to undergo reverse transcription. At this step is where NRTIs will disrupt the copying process by blocking the reverse enzyme transcriptase, and NNRTIs drug molecules will attach themselves to reverse transcriptase to inhibit copying the RNA strand. Once the reverse transcription is finished, the RNA begins forming the pre-integration complex (PIC). The PIC is then translocated into the nucleus to integrate itself into the host DNA. It is transcribed and translated to form new viral RNA and proteins. Integrase inhibitors work at this step to prevent the PIC from integrating with the host cell's DNA. Ultimately, the new viral RNA and proteins formed are subsequently translocated to the cell surface to assemble into new immature virus forms. The new viruses bud off of the cell membrane and are released. Finally, during maturation, the protease enzyme cleaves the polyprotein to form mature Gag proteins, resulting in new infectious virions [1]. During this step, protein inhibitors prevent the virus from maturing by interrupting the new virus particle's assembly. However, despite the advanced clinical research of the virus's life cycle and current treatment options available, there are still various challenges.

Challenges in Current Antiretroviral Treatment

One of the main challenges faced in current antiretroviral treatment is poor patient compliance. With the need for patients needing to take their medication daily for a lifetime, some

patients fail to adhere to their treatment schedule. Noncompliance results in ineffective drug levels within their body and the rapid rebound of viral replication [10]. Additionally, due to the high genetic diversity and continuous mutations of the virus, some patients may develop resistance to particular combinations of drugs even with compliant adherence. Patients also face side effects due to toxicities of antiretroviral drugs such as increased rates of heart disease, diabetes, liver disease, and many forms of cancer in aging HIV-infected patients who have been receiving treatment [11]. Whether these side effects are due to long-term HIV infection, drug regimens, or both, is uncertain. Finally, maintaining and sustaining HIV treatments is costly as this affects millions of people across the globe.

Even more pressing, under current treatment, complete eradication of the virus has not been possible. The leading cause for this is that HIV resides in 'latent reservoirs' within memory $CD4^+$ T cells and cells of the macrophage-monocyte lineage [10]. Macrophages have been found to significantly contribute to the generations of elusive mutant genotypes of the virus as it serves as the host for viral genetic recombination [11]. HIV-1 infection remains persistent in reservoir organs within the body that does not allow anti-HIV drugs' easy penetrance. This poses a challenging situation for patients as eradicating the virus in these reservoir organs is critical to their successful long-term treatment. Cells that harbor latent HIV-1 are typically concentrated in reservoir organs in the body, such as secondary lymphoid tissue, testes, liver, kidney, lungs, gut, and the central nervous system (CNS) [10].

The Effects of HIV-1 on the Central Nervous System

The CNS is one of the main targets for HIV-1 infection as HIV-1 is a neurotropic virus that causes inflammatory and neurotoxic host responses [12]. HAND (HIV-1 associated

neurological disorders) is the most common manifestation of HIV-1 pathogenesis within the CNS. HAND is characterized by a range of development of cognitive, motor, and behavioral impairments such as impaired short-term memory, impaired decision making, lack of coordination to progressive dementia [12]. HAND occurs in three different classifications: asymptomatic neurocognitive impairment, mild neurocognitive disorder, and HIV-associated dementia, which is the most severe category [13]. While cART regimens have effectively reduced HAND in patients, the prevalence of HAND increases as HIV/AIDS patients live longer [12]. Even in the era of current ART, HIV-1 may cause cognitive, behavioral, and motor difficulties in 40-60% of infected individuals and vary in severity [13].

Microglial cells are significant cellular reservoirs of latent HIV-1 and are involved in HAND development and progression [14]. Resting microglial cells are transformed into an activated macrophage-like state when they sense a change in their microenvironment. When activated, these cells release several cytokines, chemokines, and other neurotoxic proteins; these factors contribute to the pathological neuroinflammation observed in HAND [14]. Clearing infected microglial cells are critical to achieving the eradication of HIV-1.

While the CNS has developed a series of barriers to protect itself from invading pathogens, neurotoxic molecular substances, and circulating blood cells, the blood-brain barrier (BBB) is the most extensive and elusive [15].

The Blood-Brain Barrier

The BBB is a diffusion barrier essential for the normal function of the CNS as it functions as a protective, selectively permeable membrane that protects the brain from foreign substances such as infectious agents and neurotoxic substances [13]. Additionally, the BBB is a

regulator of energy metabolites, specific ion channels, and transports. Essential molecules such as water, glucose, amino acids, and some lipid-soluble molecules are required for neuronal growth and function to pass through the BBB through passive diffusion and selective transport mechanisms [13].

The BBB composition comprises specialized microvascular endothelial cells, highly connected by adherents and tight junctions, and a sparse layer of pericytes [15]. The endothelium is also surrounded by a basement membrane, a layer of astrocyte end-foot process, and neurons and microglia that act as essential mediators of BBB integrity in physiological conditions [15]. With its overall cellular architecture, the BBB possesses very low and selective paracellular permeability, making it a tremendously difficult barrier for any drug to cross [13, 16].

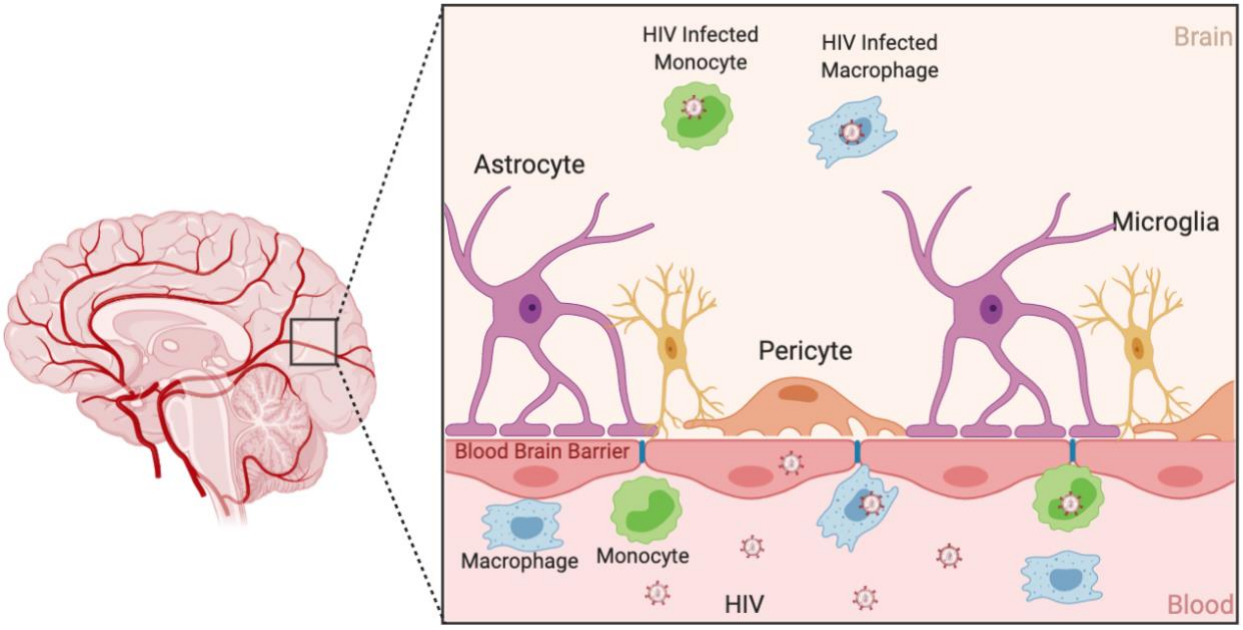

Figure 2: Schematic overview of HIV-1 infection within the BBB. *The BBB comprises closely packed brain microvascular endothelial cells surrounded by macrophages, microglia and foot processes of astrocytes to protect the brain; however, HIV-1 can bypass the barrier. HIV-1 is*

introduced into the CNS as a passenger in cells that traffic across the BBB and cause infection within the brain. Figure adapted from BioRender.com.

Although there is a robust and cohesive system among the tightly connected endothelial cells, the BBB allows for the selective passage of cells and small molecules to the brain [13, 15]. The most widely recognized model for how HIV-1 is introduced into the CNS through the BBB is known as the "Trojan Horse hypothesis". Based on this model, HIV-1 can cross the CNS as a passenger in cells trafficking the brain, such as macrophages (Figure 2) [13]. HIV-1 infects several CD4+ cells, such as T cells and monocytes, and these cells circulate within the blood, cross the BBB, and cause infection within the CNS [13].

As forementioned, considerable evidence suggests that microglial cells, CNS resident macrophages, constitute a significant cellular reservoir in the brain. Previous research indicates that infected CD4+ T cells migrating into the brain are ingested by microglial cells, but the infection mechanism has not been demonstrated [14]. Despite the unknown infection mechanism, it is clear that microglial brain cells are permissive to HIV-1 infection. Evidence supports that microglial cells are infected by HIV-1 both *in-vitro* and *in-vivo* [17]. Unlike other potentially infected cells in the brain, microglial cells have a slow turnover and long half-lives, thus allowing the persistence of HIV-1 in the brain throughout a patient's life [14]. Microglia can become latent viral reservoirs due to a few key features. When infected, microglia are far more resistant to the virus's cytopathic effects. Unlike CD4+ T cells, microglia are non-lytic and are resistant to apoptosis [14].

Upon finding the host cell's nucleus, the HIV-1 genome encodes for polyproteins (*Gag, Pol,* and *Env*), subsequently proteolyzed into individual proteins [13]. *Env* encodes for a glycoprotein, gp120, found on the virion surface, a potent neurotoxin, causing neurotoxicity even

in pico-molar concentration [13]. Studies have shown that gp120 induces oxidative damage and production of reactive oxygen species (ROS) within the BBB's endothelial cells, which leads to alteration of the BBB integrity by increasing permeability and susceptibility [18]. Loss of BBB integrity may manifest in various ways, such as leakage of blood components into the brain parenchyma, loss of key protein components of endothelial cell tight junctions, and loss of vessel structural proteins [18]. Serum leakage across the BBB occurs in the brains of patients with HIV-associated dementia. The accumulation of serum proteins in neurons and glial cells has been observed more frequently in HIV-1 positive patients with dementia than those with no cognitive impairment [18]. The BBB's inaccessibility allows for persistent HIV infections and inflammation within the CNS and remains a significant hindrance for inhibiting HIV replication within the brain.

Due to its restrictive nature, drug delivery to HIV-1 residing within the brain remains an obstacle; hence, treatments for CNS diseases are limited. A research study observed that *in-vivo* brain concentrations of ART drugs in mice were 10 to 100-fold less in brain tissues than plasma and liver levels after 4 hours of post-drug administration [19]. However, despite the low drug concentration in the brain, the experimental ART drugs suppressed HIV-1 infection but patients still had a detectable HIV-1 in the brain; which suggest that viral suppression in feasible but new approaches to enhance ART efficacy are required for HIV-1 eradication in the brain [19]. Therefore, cART needs to have improved CNS penetration methods for effective treatment and prevention of HAND, such as developing a new delivery system for antiretroviral drugs that can successfully penetrate the BBB and inhibit HIV replication and reduce viral load. [12]

Nanotechnology used as Pharmaceutical Carriers

In the last decades, nanotechnology has been shown to bridge the barrier of biological and physical sciences by applying nanostructures and nanophases to various fields of science, specifically in nanomedicine and nano-based drug delivery systems [20]. Nanotechnology utilizes nanomaterials with sizes ranging between 1 and 100 nm. The small size of these nanostructures makes them favorable for applying cell-based antiretroviral therapies. they can be effectively delivered to micron sized cells that can sustain drug release in active viral replication [4]. The application of nanotechnology to medicine is most often known as nanomedicine and involves using these nanoscale materials for preventative, therapeutic, and diagnostic purposes [10]. Nanostructures can be utilized as delivery agents by encapsulating drugs or attaching medicinal drugs, enabling them to be delivered to targeted tissues more precisely with a controlled dosage release [20]. The central concept surrounding nano drugs revolves around developing a "target specific, effective, safe, and controllable" drug delivery method [16]. Drugs with very low solubility that can depend on lipophilicity have various biopharmaceutical delivery issues, including limited biological accessibility after intake through the mouth, less diffusion capacity, and more quantities for intravenous intake [20]. Most of the 25+ antiretroviral drugs approved by the FDA for oral administration have low solubility in water due to their lipophilic nature, limiting the rate and extent of drug absorption [21]. However, nanomedicine represents an excellent strategy to overcome conventional drug delivery systems [20, 22].

Ultimately, a nano carrier-based delivery system can be utilized to achieve better drug pharmacokinetics, improved efficacy, and safety [22]. Several important properties of nanoparticles (NPs) are desirable for drug delivery vehicles, such as high biocompatibility, long *in-vivo* circulation half-life, and high loading drug/diagnostic capacity. Significant attention has

been drawn to a variety of nanocarriers, such as solid lipid NPs (SLN) [23], liposomes [24], polymeric micelles [25], dendrimers [26], oil bodies [27], aptamers [28], and nanoporous lipid bilayers [29], demonstrating great potential for *in-vivo* applications [25, 30, 31]. Recently, a study has successfully designed a dendrimer for targeted drug delivery to increase the biocompatibility and specificity of tissue distribution of anti-HIV drug, zidovudine [32, 33]. The study demonstrated that the dendrimers greatly increase zidovudine concentration in lymph nodes with better cytotoxic profile than the free drug [33]. The overall goal of utilizing a nano-formulated drug delivery system is to treat a disease with minimum side effects.

One of the most widely used delivery vehicles for carrying agents are liposomes. Liposomes have several advantages over other nano delivery systems by being less toxic and capable of having a high therapeutic index. They are composed of a lipid bilayer in a spherical shape that is made up of amphipathic phospholipids consisting primarily of phosphatidylcholines (PC) that encapsulate an aqueous core [34]. Because of their unique structure, liposomes can entrap hydrophobic agents within the lipid bilayers and encapsulate hydrophilic agents inside their aqueous center compartment [34]. Liposomes have been used as pharmacological and genetic agent carries that have advantages such as protecting drugs or other therapeutic agents from degradation, targeting to site of action through ligand peptide or antibody conjugation, and have been noted to have little toxicity or side effects [35]. Additional advantages to liposomes include a high agent-loading efficiency, high stability in biological environments, controllable release kinetics and biocompatibility [34].

Nanodiscoidal shaped bicelles or nanodisc's (NDs) share a similar chemical composition with liposomes but have not been as extensively studied. However, NDs are able to be generated with control of lipid content and particle size. A previous study has previously demonstrated that

NDs had a greater cellular uptake than their spherical counterparts [31]. This thesis will study NDs are promising nanocarriers to deliver an antiretroviral drug in an extended release.

Nanodisc and its potential

The ND comprises short and long-chain lipids and is further stabilized by polyethylene glycol-conjugated (PEGylated) lipids [31]. In the present study, ND's have been well characterized for lipid-based drug delivery to assist in entrapping drug molecules until the body has metabolized them [31]. A previous study has demonstrated that the addition of PEGylated lipids inhibits the ND from forming into multi-lamellar vesicles and is thought to be due to the steric interaction of the PEG chains that inhibits or slows the coalescence process [36]. NDs are around 30 nm in diameter and 5 nm in thickness [37, 38]. They are stable and soluble membrane mimetics, and their structure allows for additional surface/ligand modification, such as affinity tags to scaffold proteins [31].

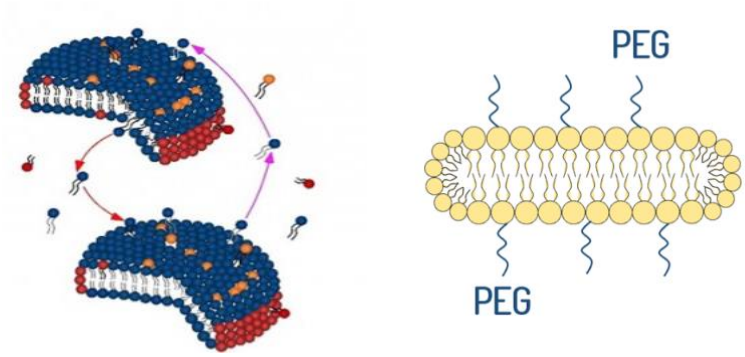

Figure 3: Model view of the nanodisc (ND)*; ND comprises short-chain and long-chain lipids and is stabilized by PEGylated lipids. NDs measure at ~30 nm in diameter and ~5 nm in thickness. Their structure allows for additional surface/ligand modification.*

An NDs efficiency strongly depends on the physicochemical characteristics of the NPs, including both size and shape. It has been established that spherical NPs with a diameter ranged

from 20 to 100 nm result in optimal tumor accumulation because of the enhanced permeability and retention (EPR) effect [39, 40]. However, different EPR effects have been reported for non-spherical nanostructures, such as nanorods, due to their differences in *in-vivo* hydrodynamic behaviors such as *in-vivo* transport and circulation extravasation into the tumor [31, 41]. For microglial cells, morphology of NPs was also seen to affect their uptake by microglia where spiky "urchin shaped" gold NPs showed a significantly greater microglial internalization compared to spherical or rod-shaped gold NPs [42, 43].

This shape effect can be seen in NDs as previous studies have demonstrated that when utilized to deliver hydrophobic molecules to cancerous cells, its cellular uptake was ~5-10 times greater than that of spherical vesicles with identical chemical composition [31, 44]. This is due to the ND taking more internalization routes than vesicles and having a larger surface-contact area for NDs to interact with the cell membrane [31]. NDs utilize two additional cellular internalization mechanisms: micropinocytosis and microtubule-mediated transport, as well as the common clathrin- and caveolae-mediated pathways (which appeared to be the only pathways utilized by nanovesicles) [44]. Additionally, bicellar NDs been demonstrated to have consistently enhanced endocytosis across three different cell lines (CCRF-CEM, KB, and OVCAR-8) compared to that of the nanovesicle [44].

this study has expanded the previous observation of ND with one of the anti-HIV drugs currently recommended by the World Health Organization (WHO), tenofovir [45]. Tenofovir (TFV) is an acyclic nucleotide analogue with a potent *in vitro* and *in vivo* antiretroviral activity; however, tenofovir has limited oral bioavailability in animals [46]. TFV is a widely used antiretroviral drug belonging to the NRTI drug class as it inhibits HIV-1 and HIV-2 DNA polymerases (reverse transcriptase) along with other viral DNA polymerases at the third main

step of HIV-1's replication cycle (Figure 1) [47]. TFV's inhibition results in DNA chain termination the impairment of viral replication [47].

As of 2019, TFV is known as one of the essential orally administered drugs in WHO's Model List of Essential Medicines [48]. TFV is generally well-tolerated by patients and is considered part of the preferred first-line ART regimen by WHO for ART-naïve adults and adolescents and is typically used in combination with other anti-HIV medications, most notably with dolutegravir, lamivudine and efavirenz [45]. TFV has been approved to treat HIV and HBV infection [16, 49]. TFV, combined with another NRTI drug, emtricitabine, is currently approved for pre-exposure prophylaxis (PrEP) for individuals at high risk of contracting HIV [49]. While TFV is typically used in combination with other antiretrovirals, this study will look into encapsulating TFV, as a model drug, into the ND as a proof of concept that could apply to other drugs in the future.

TFV exists as a dianion compound which makes it very polar. By being such a polar species, TFV does not readily undergo passive diffusion across cellular membranes, resulting in low bioavailability after oral administration [47]. TFV has been found to cross the blood-cerebrospinal fluid barrier but cannot readily cross the BBB to reach deep brain sites due to its hydrophilic nature [46]. Therefore, this study looked into a ND based drug delivery that could be used as a potential method to deliver extended-release of TFV for long-term inhibition of HIV-1 within the brain. The nanodisc was developed and characterized by TFV encapsulated within the ND structure. Two different drug-to-lipid ratios of 1:20 ND and 1:4 NDwere observed for their biological safety sustained-release properties.

Objectives

The specific aims of this Master thesis were as follows:

Specific Aim #1: To characterize and evaluate the biological safety of the nanodisc formulation.

The first aim of this thesis was to characterize and screen the ND formulation in the biological systems via *in-vitro* conditions for cytotoxicity or cellular inflammatory responses. The TFV loaded NDs were synthesized and prepared at varying drug-to-lipid ratios with PEGylated lipid chains to help stabilize the ND. ND formulations were then characterized and evaluated for chemical structure, size, shape, morphology and polydispersity by molecular lipophilic surface potential (MLSP) modeling, dynamic light scattering (DLS), and small-angle X-ray scattering (SAXS). Cell viability analysis of ND treated microglial and neuronal cells was determined by 3-(4,5-dimethylthiazol-2-yl)-5-(3-carboxymethoxyphenyl)-2-(4-sulfophenyl)-2H-tetrazolium, inner salt (MTS) assay. Cellular inflammatory response of the ND was evaluated by a reactive oxygen species (ROS) assay.

Specific Aim #2: To determine the sustained-release properties of the nanodisc and liposome formulation.

The second aim of this thesis aim is that the ND and liposome formulations would effectively perform sustained-drug release properties. An *in-vitro* extended drug release study was utilized to study the sustained drug release profiles of the ND and liposome formulations using an equilibrium dialysis system in phosphate buffer saline (PBS). The ND was further investigated for its drug delivery properties to cross the blood-brain barrier (BBB) by setting up an *in-vitro* BBB model to mimic the biological barrier. The intracellular uptake of the ND by

microglial cells. A maximum tolerated dose (MTD) study and pharmacokinetic (PK) study was performed on mice to evaluate the ND's biological safety and sustained drug release *in-vivo*.

CHAPTER II

METHODOLOGY

Preparation of Nanodisc and Liposomes

All solvents (methanol, ethanol, chloroform, and toluene) were purchased from Sigma-Aldrich and filtered with a 0.2 μm filter before use. Zwitterionic long-chain dipalmitoylphosphatidylcholine (di-16:0, DPPC), charged long-chain dipalmitoyl phosphatidylglycerol (DPPG), zwitterionic short-chain dihexanoyl phosphatidylcholine (di-6:0, DHPC), and polyethylene glycol (PEG2000)-conjugated distearoyl phosphoethanolamine (DSPE-PEG2000) were purchased from Avanti Polar Lipids (Alabaster, AL, USA) and used without further purification. TFV, DiR dye, phosphate-buffered saline (PBS), and all pharmacological inhibitors were purchased from Sigma-Aldrich (St. Louis, MO).

NDs were prepared via self-assembly, as previously described [36, 50]. The lipids or lipids + drugs at desired ratios were homogenized in a solution of chloroform and methanol (13:7). The organic solvents were dried through a nitrogen purge at 55 °C and desiccated at room temperature overnight in a vacuum oven to remove any residual solvent. The dry lipid or lipid + drug mixtures were homogenously hydrated with filtered deionized water to 10 wt.% through temperature cycling and vortexing. The experiments were performed with the samples diluted to 1.0 or 0.1 wt.%. The drug-loaded nanodiscs were further centrifuged at 5000 rpm for 10 minutes to separate the unencapsulated drugs and large drug/lipid complexes. The experiments were

performed with the samples diluted to 1.0 or 0.1 wt.%. The drug-loaded NDs were further centrifuged at 5000 rpm for 10 minutes to separate the unencapsulated drugs and large drug/lipid complexes. The lipid composition remains constant throughout the samples (DPPC:DHPC:DPPG:DSPE-PEG2000 = 66.6:25.1:3.8:3.8) drug-to-lipid molar ratios studied were 1:20 and 1:4. Drug-to-lipid ratios are considered theoretical and based on how much lipid and drug is being used in the whole solution, which can be calculated to know the amount of lipid and drug to add.

Liposomes are formed in a similar process as the NDs but can transform into vesicle shaped through a prolonged incubation (48 hours). A disc-to-vesicle structural transition occurs as the long-chain lipid undergoes from the low-temperature gel (order) to high-temperature L_a (liquid disorder) phase. Both nanodiscs and liposomes exhibit uniform dimensions. At low lipid concentrations, the liposomes irreversibly form and do not revert to nanodiscs even when the long-chain lipid becomes gel phase at a lower temperature [38, 51, 52]. These properties allowed us to produce different low-polydispersity morphologies from mixtures of identical chemical compositions [38].

Computational molecular modeling and calculations

Molecular simulation studies were carried out to understand the interactions between the two drugs and the lipid molecules. The molecular lipophilic surface potential (MLSP) and molecular electrostatic potential (MEP) of TFV were investigated using VEGA-ZZ 3.2.0 software. MEP depicts the 3D charge distributions of the molecules. MLSP simulates the combined lipophilicity of a molecule's fragments at given points in space using the Molinspiration Property Calculation Service molecular [53] based on the Gasteiger–Hückel

charges of the atoms [54, 55]. The color ramp for the MLSP ranges from violet/blue (higher lipophilicity or more significant lipophilicity potential (LP) to red (lower lipophilicity or lower LP).

Small- and wide-angle x-ray scattering (SAXS and WAXS)

SAXS/WAXS was used to analyze the nanostructure of the NDs. Before measurements, samples were ultra-sonicated in a water bath for 30 min and vortexed for 10 minutes. All samples were tested at lipid concentrations of 10 mg/mL. SAXS/WAXS measurements were conducted at 16ID-LiX Beamline at National Synchrotron Light Source II, located at the Brookhaven National Laboratory (Upton, NY), using the standard flow-cell-based solution scattering setup with x-ray energy of 13.5 keV. The SAXS/WAXS intensity is expressed as a function of the scattering vector, q ($q \equiv \frac{4\pi}{\lambda} sin\frac{\theta}{2}$, where θ is the scattering angle) varies from 0.005 to 2.5 $Å^{-1}$ [56]. Radial averaging and q-conversion of data were performed using the standard software [57] by merging the data collected from all three detectors in the measurements. The transmission correction and background subtraction were performed to minimize the hydrogen bond's intensity from water at ~ 2.0 $Å^{-1}$.

Dynamic light scattering (DLS)

Size and population distribution of the nanocarriers were determined by ALV/CGS-8F/4 (ALV compact goniometer system, Germany) instrument equipped with a 632.8 nm laser beam. The samples were dissolved in ultrapure distilled filtered water to 0.1 wt. % and vortexed before each measurement. The results were the average of 10 times measurements.

Zeta Potential

The Zeta potential is measured within 30 minutes of sample preparation in PBS. The measurements are recorded in triplicate, and the averages of the results are used for data representation purposes using a 90Plus Particle Size Analyzer (Brookhaven Instruments Corporation, Holtsville, NY, USA).

Microglia and Neuroblastoma Cell Culture

Human embryonic microglial clone 3 cells (HMC-3) and human neuroblastoma cells (SH-SY5Y) were purchased from the American Type Culture Collection (ATCC) Manassas, VA, USA). The transformed cell lines retain the properties of primary cells. They represent homogeneous cell populations that can be grown indefinitely and might represent a convenient system for their functions' biochemical analysis. Cells were cultured in Eagle's Minimum Essential Medium (EMEM) (ATCC®, Manassas, VA, USA) supplemented with a fetal bovine serum to a final concentration of 10% at 37°C in a humidified, 5% CO_2 atmosphere as recommended by the supplier.

Cell viability assay of ND

The nanodisc's cell viability was determined via a 3-(4,5-dimethylthiazol-2-yl)-5-(3-carboxymethoxyphenyl)-2-(4-sulfophenyl)-2H-tetrazolium (MTS) assay on HMC-3 and SH-SY5Y cells. Cells were cultured in 96-well black bottom plates at 50,000 cells per well and incubated at 37°C in a humidified, 5% CO_2 atmosphere for 24 hours to allow for 70% confluence. [58]. After 24 hours, cells were treated with various nanodisc concentrations (0.005-

0.2 mg/mL) for 72 hours. The same concentration of unformulated TFV (Sigma Aldrich, Milwaukee, WI, USA) (also called free drug or FD-TFV) was also measured in similar conditions simultaneously. Untreated cells incubated with solely fresh growth medium were considered as controls. After incubation, cells were washed and incubated with 100 µl of fresh respective growth medium. Cells were incubated with 20 µl of MTS reagents (CellTiter 96® AQueous One Solution; Promega) along with the 100 µl of cell media for 1 hour at 37°C in a humidified, 5% CO_2 atmosphere. After incubation, absorbance readings at 490 nm were taken using a BioTek Synergy HTH.T. multi-mode microplate reader (BioTek, Winooski, VT, USA) every hour following for 4 hours for a total of five measurements. MTS assay was performed and optical density of culture supernatant was measured at 490 nm The net absorbance (Sample Absorbance – Absorbance of Blank) was taken as an index of cell viability of treated and untreated cells. All measurements were taken as three independently replicated experiments of give values each. Cell viability was calculated as the following equation: $\frac{Sample}{Control}$x 100%.

Reactive Oxygen Species of ND

Reactive oxygen species (ROS) productions in HMC-3 and SH-SY5Y cells following nanodisc treatment were detected using dichlorofluorescein diacetate assay (DCF-DA; Molecular Probes, Eugene, OR). Cells were cultured in 96-well black bottom plates at 100,000 cells per well and incubated at 37°C in a humidified, 5% CO_2 atmosphere for 24 hours to allow for 70% confluence. The following day, cell media was taken out from each well and replenished with 100 µl of PBS + 1% FBS. Pre-assigned negative control cells were treated with antioxidant catalase, and the plate was incubated for 2 hours. After incubation, cell media was taken out and replenished with 100 µM dichlorofluorescein diacetate assay (made with PBS + 1% FBS) to

each well and incubated for 1 hour. Following incubation, cells were treated with various concentrations (0.01-0.1 mg/mL) of the nanodisc and incubated for 2 hours. A study of FD-TFV was also measured in similar conditions simultaneously. Cells with no drug (untreated) were incubated with a growth medium and considered the control. Cells were also treated with H_2O_2 (50 µM) as triplicates positive controls. Following 2 hours, the first reading of cell ROS production was read in a BioTek Synergy HTH.T. multi-mode microplate reader (BioTek, Winooski, VT, USA) and then taken every hour for the following 18 hours (excitation 485 nm and emission 528 nm; BioTek). All measurements were taken as three independently replicated experiments of give values each.

In-Vitro Sustained Drug Release Assay of ND

The drug release kinetics of the nanodisc-based drug delivery was determined in PBS using equilibrium dialysis. A 50 µL solution of the 5 mg/mL nanodisc formulated TFV along with 1 mL of PBS was placed into a dialysis bag (Pur-A-Lyzer™ Maxi 6000 Dialysis Kit, SIGMA with a molecular cutoff: 6-8 kDa), sealed, and put into a 50 mL conical tube filled with 20 mL of PBS with a composition of 0.1% Tween 20 aqueous solution. The tube was then placed on a 37°C shaker and rotated at 150 rpm. At the following scheduled intervals (0 minutes, 5 minutes, 10 minutes, 15 minutes, 30 minutes, 60 minutes, 2 hours, 4 hours, 8 hours, 1 day, 2 days, 4 days, 6 days, 8 days, 10 days, 12 days, and 14 days), 200 µl of the release medium was collected for liquid chromatography-tandem mass spectrometer (LC-MS/MS). immediately after that, 200 µl of fresh dissolution medium (PBS) at 37°C was replenished. Samples were collected as triplicates. The exact concentration of FD-TFV was used as a control.

TFV was monitored by LC-MS/MS using an AB Sciex (Framingham, MA) 6500+ QTRAP® mass spectrometer coupled to a Shimadzu (Columbia, MD) NexeraX2 LC. TFV was measured with the mass spectrometer in positive MRM (multiple reaction monitoring) modes by following the precursor to fragment ion transitions 288.1 to 176.2. A Kinetex C8 column (5 micron, 100 X 4.6 mm) was used for chromatography with the following conditions: Buffer A: dH20 + 0.1% formic acid, Buffer B: acetonitrile + 0.1% formic acid, 0 - 1.0 min 5% B, 1.0 – 3.0 min gradient to 100% B, 3.0- 5.0 min 100% B, 5.0 – 5.1 min gradient to 5% B, 5.1 – 6.0 5% B. Indinavir (transition 614.6 to 138.9) was used as an internal standard (IS). 50 µl of the provided sample was mixed with 100 µl of 50:50 methanol:0.02N HCL containing 50 ng/mL Indinavir IS. Samples were vortexed for 15 sec, incubated at room temp for 10', and spun at 16,100 x g 4ºC in a refrigerated microcentrifuge. LC-MS/MS then evaluated the supernatant. Standard curves were generated using PBS spiked with varying concentrations of TFV or TDF and processed as described above. The concentration of drug in each timepoint sample was quantified using Analyst 1.7 software (AB Sciex). A value of 3-fold above the signal obtained from blank PBS was designated the limit of detection (LOD). The limit of quantitation (LOQ) was defined as the lowest concentration at which back -calculation yielded a concentration within 20% of theoretical and above the LOD.

Drug Release of ND *In-Vitro* Environment through the BBB

Primary Human Brain Microvascular Endothelial Cells (HBMVEC) and human astrocytes (HA) (ScienCell Research Laboratories, Carlsbad, CA) were obtained and prepared for plating of the BBB model. *In-vitro* BBB model was established in a transwell plate as per published protocol [59, 60]. HA was split and seeded on the lower side of a 0.4 um pore size

PTFE membrane tissue culture inserts at an initial concentration of 10^5 cells per well. HBMVEC was incubated for 2 hours to allow cells to be saturated on the outside of the insert. After incubation, a confluent layer of HBMVEC was grown on the upper side of the membrane. Following 24 hours of incubation, the BBB's integrity was measured with transendothelial electrical resistance (TEER) using Millicell ERS microelectrodes. Typical TEER values of untreated BBB were observed to be around ~140 Ω/cm^2. Cells were allowed to grow up to 70% confluency, and the pre-determined concentration of ND was introduced into the upper chamber of the transwell insert. Following the introduction to the upper chamber, media was collected at various time points (30 minutes, 1 hour, 1 day, 2 days, 4 days, 6 days, 8 days, and 10 days) from the lower chamber and replenished fresh media. Samples were taken as triplicates for each treatment. The samples were stored at -20°C until further analyses. The drug content from the collected media samples with same conditions as forementioned above. Additionally, TEER measurements were performed at 24 hours post-treatment and at each time point collection. Simultaneously, a separate set up with the same concentration of FD-TFV was used as a control.

Cell Uptake and Characterization of Extended-Release from ND

Microglial uptake, retention, and release of 1:20 ND, 1:4 ND, and FD-TFV were determined as previously described protocol [61, 62]. HMC-3 cells were cultured in 24-well at 50,000 cells per well and incubated at 37°C in a humidified, 5% CO2 atmosphere for 24 hours to allow for 70% confluence. After 24 hours of cell growth, samples were assigned into different treatment groups of 1:20 ND, 1:4 ND, and FD-TFV and treated at 0.0625 mg/mL concentration. Following drug treatment, samples were incubated at 37°C, and cell uptake was determined every hour over 8 hours and at a 24-hour timepoint. For each sample, media was collected into

microcentrifuge tubes and stored at -20°C for later analysis. Samples were taken as triplicates for each treatment. Cells were trypinized and centrifuged to collect pellets. Cell pellets were then stored at -20°C for later analysis.

Cell pellets were washed in 1 mL of PBS and centrifuged at 3,000 rpm for 8 minutes at 4°C. PBS was then discarded, and cell pellets were resuspended in 200 uL of HPLC-grade methanol, homogenized, and centrifuged at 14,000 rpm for 10 minutes at 4°C. The methanol extract was then collected into a separate microcentrifuge tube, and cell debris/pellet was discarded. Samples were then placed into a speed vac at 60°C (Eppendorf Vacufuge Plus, Hauppauge, NY) to dry out samples. Samples were then stored at -20°C for later analysis and resuspended with 50 uL of PBS for analysis.

In-Vivo Maximum Tolerated Dose Study and Pharmacokinetic Analysis of ND

Eight-week-old, healthy BALB/c mice (1:1 male and female) were purchased from Charles River Laboratories (Hollister, CA) and housed under a 12-hour/12-hour light/dark cycle. An Envigo Teklad Certified Global 18% protein rodent diet, #2018C, and water were provided to the mice ad libitum. Mice were administered a single dose intravenous (iv) dose administration. The average weight of Phase A and Phase B mice were 17.3 - 18.6 g and 17.2 - 23.4 g, respectively. All procedures were per the current Association for Assessment and Accreditation of Laboratory Animal Care (AAALAC) recommendations. *In-vivo* studies were carried out in collaboration with NIH-DAIDS Preclinical Contract Services.

This *in-vivo* study was set up into two phases: Phase A was performed to determine the maximum tolerated dose (MTD study), and Phase B was performed to determine the plasma

pharmacokinetics (PK study) of two formulations of TNF (ND and a saline preparation) following an iv dose administration.

Table 1: MTD Study groups and their associated treatments

Group [a]	Treatment	Dose Route	Dose Level (mg/kg)	Dose Conc. (mg/ml)	Dosing Volume (ml/kg)	No. of Animals	Drug to Lipid Ratio [b]
1	Bicelle [c]	iv	0	0	4	2M/2F	0
2	tenofovir	iv	2	0.95	2.1	2M/2F	1:20
3	tenofovir	iv	10	2.50	4	2M/2F	1:7.3
4	tenofovir	iv	15	3.75	4	2M/2F	1:5
5	tenofovir	iv	20	5.00	4	2M/2F	1:3.8

[a] All animals were treated on Day 1 and observed for up to 48 hr. There was a 30-45 min time interval between each dose group to observe the treated animals. Surviving mice from each dose group were euthanized ~48 hr postdose; necropsies were not performed on the mice.
[b] Each dose group had a lipid concentration of 5%.
[c] Bicelle = lipid; 5 mg/100 µl

For the MTD study, ten males and ten females used for this phase were divided into five different treatment groups (Table 1). There were 30-45 minutes time intervals between the dose groups, and mice were observed immediately postdose, 30-45 minutes postdose, and once daily up to 48 hours for toxicity signs. Animals were monitored for any altered clinical signs such as gross motor and behavioral activity and any observable appearance changes.

Table 2: PK study groups and their associated treatments (ND and FD-TFV)

Group	Treatment [a]	Dose Route	Dose Level (mg/kg) [b]	Dose Conc. (mg/ml) [b]	Dosing Volume (ml/kg)	No. of Animals [c]	Blood Collection Times (hr) [d]
6	Tenofovir (in lipid formulation)	iv	20	5	4	12M/12F	0.167, 0.5, 1, 3, 8, 24, 48 and 72
7	Tenofovir (in sterile saline formulation)	iv	20	5	4	12M/12F	0.167, 0.5, 1, 3, 8, 24, 48 and 72

[a] Two different dose formulations were used in Phase B.
[b] Dose level and dose concentration was selected based on the MTD (Phase A) results and in consultation with the Sponsor.
[c] Blood was collected from 3 untreated mice per gender for baseline control samples.
[d] Two blood samples were collected from each mouse; the last sample was a terminal bled; three mice per gender were assigned for each time point. Blood was processed to plasma.

During the PK study, 24 males and 24 females used for this phase were divided into two groups (Table 2). Two-dose formulations of TNF were used in this phase as a single iv dose administration; the ND supplied at 5 mg/mL (Group 6) and a freshly prepared TNF saline solution at 5 mg/mL (Group 7). Additionally, six untreated mice were used to compare as baseline samples. Blood was collected for drug plasma levels at 0.167, 0.5, 1, 3, 8, 24, 48, and 72 hours postdose. Animals were observed immediately postdose, once daily, and before the last blood collection. PK data analysis was performed using the plasma concentrations of TNF via LC-MS/MS.

All reagents used in the plasma samples analysis were either HPLC-grade or American Chemical Society (ACS) reagent grade. CD-1 mouse plasma collected with K3 EDTA anticoagulant was purchased from BioIVT (Westbury, NY). The test article Tenofovir (the monohydrate form) was supplied by US Pharmacopeia. Medical Isotopes, Inc supplied the standard internal Tenofovir-d6, and the purity was assumed to be 100% during stock solution preparation. Calibration standards, quality control samples, blank plasma samples, and the study samples were placed into microcentrifuge tubes and spiked with an internal standard spiking

solution (except the blank plasma samples). Samples were briefly vortexed before centrifugation. Following centrifugation, the supernatant was transferred into glass autosampler vials containing Milli-Q water and briefly vortexed. Samples were then stored into a refrigerated autosampler (set at 5°C) before injection into the LC-MS/MS system.

TFV was detected with the mass spectrometer in positive MRM (multiple reaction monitoring) mode by following the precursor to fragment ion transitions 288.1 to 176.2 for TFV. A Phenomenex Synergi Polar-RP column (4 microns, 100 X 2 mm) was used for chromatography with the following conditions: Buffer A: 2% acetic acid in water, Buffer B: 0.1% acetic acid in acetonitrile, 0 - 2.0 min 2% B, 2.0 – 2.01 min gradient to 98% B, 2.01- 3.5 min gradient to 98% B, and then 3.51 – 5 min gradient to 2% B. The concentration of drug in each timepoint sample was quantified using Analyst 1.7 software (AB Sciex).

Statistical Analysis

Experiments were performed in multiple replicates with data presented as mean ± SEM. Each experiment's statistical significance was analyzed by one-way ANOVA or two-way ANOVA test with posthoc Dunnett's multiple comparisons test by GraphPad Prism software (GraphPad Prism Software Inc., San Diego, CA). P-values of ≤ 0.05 were considered significant.

CHAPTER III

RESULTS

Computational molecular modeling and calculations

There are several challenges in developing long-acting nanoformulation for anti-HIV drugs. In this regard, the approach used within this project for an ND-based formulation has shown significant advancement in the drug delivery approach. The initial characterization with molecular lipophilic surface potentials (MLSP) modeling results for TFV showed lower lipophilic locations surrounding the drug molecule (Figure 4). The analysis provided the lipophilic potential for atoms or groups of atoms and the 3D spatial features of the molecular interactions within the drug molecule. The nanodisc is a low-polydispersity, spontaneously-forming discoidal shape with a diameter of about ~30 nm and a thickness of ~5 nm. The nanodisc is composed of long-chain lipids, dipalmitoyl phosphocholine (DPPC), short-chain lipids, and dihexanoyl phosphocholine (DHPC). Additionally, nanodiscs are capable of entrapping hydrophobic molecules and having a robust formation and assembly mechanism. The nanodisc represents an attractive drug delivery model to bypass the blood-brain barrier inhibiting HIV-1 replication within the brain.

The molecular electrostatic potentials (MEP) and MLSP of TFV were calculated using the VEGA-ZZ software. MEP illustrates the 3D charge distributions within molecules, and MLSP demonstrates the lipophilicity potential in the different regions of the molecules. MEP and MSLP provide insights into the molecular structure, lipophilicity, and surface charge of the drugs and characterize TFV interactions with the phospholipids and their entrapment within the NDs. Furthermore, both MLSP and MEP are valuable tools for understanding the self-assembly process of drug-loaded NDs and encapsulation. As shown in Figure 4, TFV is a highly lipophobic molecule (shown in red/orange), limiting its incorporation within the bicellar core. TFV prefers to locate in the external terminals of the phospholipids due to their higher hydrophilicity.

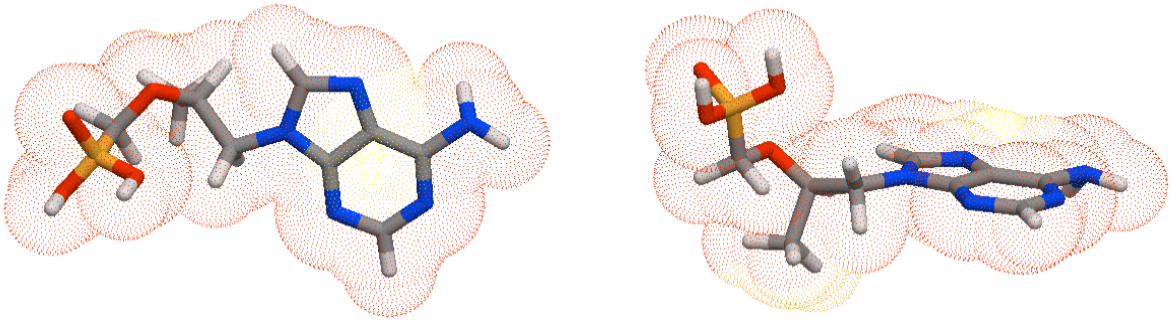

Figure 4: MLSP modeling of antiretroviral drug, tenofovir (TFV)*; MLSP provided insights into the drug molecule's lipophilicity to help characterize TFVs interactions within the ND. The low lipophilic locations within TFV (red/orange) limits TFVs ability to be incorporated within ND core.*

Structural Characterization

The size distribution of drug-loaded NDs was also investigated using dynamic light scattering (DLS). The hydrodynamic radius (R_h) of the NDs using DLS in an aqueous solution was used to determine the pristine and drug-loaded NDs' size distribution. In the pristine NDs without any drugs, R_h was approximately 8.5 nm. The hydrodynamic radius, R_h of NDs was 10 ~ 13 nm. After drug encapsulation and at lower drug concentrations (drug: lipid ratios of 1:20), a slight increase in size was observed which can be observed in group 2's broader peak. Larger aggregates of the ND sample were observed within the sample but are considered as the minority and are observed as 1 in 10,000 particles. The DLS results confirmed the uniformity of the nanodiscs for individual TFV-ND samples.

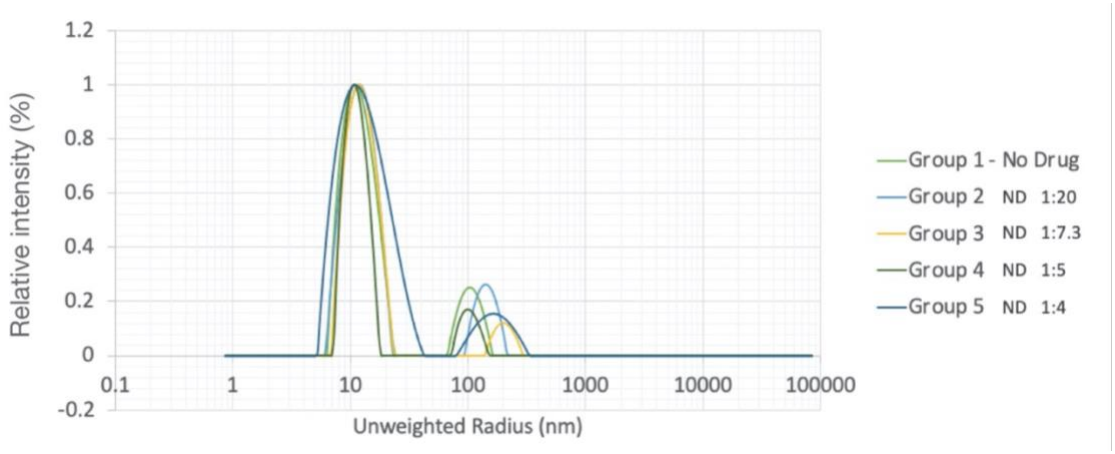

Figure 5: DLS of NDs at varying drug-to-lipid ratios; *DLS was used to determine the size distribution within the solutions. Results demonstrated the hydrodynamic radius of the ND ranged from ~10-13 nm and confirmed the uniformity of the NDs.*

SAXS was used to provide the detailed discoidal core-shell architecture of the designed ND (Figure 6). This particular technique is sensitive to the electron density distribution in the structure of nano-assemblies averaged in time. The pattern of the x-axis is 1/Angstrom; thus,

higher x-values correlate to smaller distances. Lipid bilayers within the nanodisc are considered as the lipophilic core, represented in SAXS data as hydrocarbon chains, being sandwiched between two shells of hydrophilic phosphatidylcholine head groups outside. Since the phosphate group has the highest electron density in the system and is higher than hydrocarbon tails and water, the electron density profile across the bilayer can be approximated by a "square well." Moreover, the slope at the low q region could also infer the lipid aggregates' possible morphology.

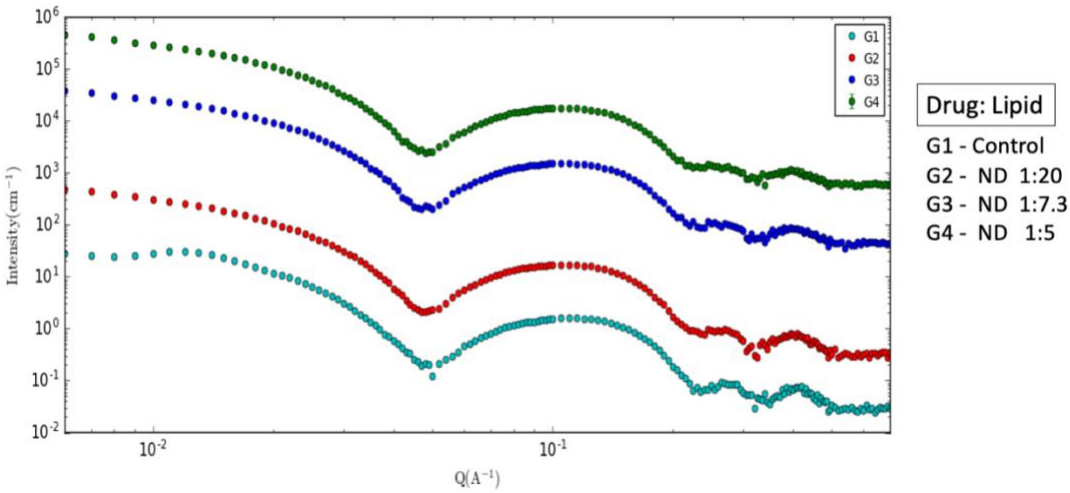

Figure 6: SAXS graph of NDs at varying drug-to-lipid ratios; *SAXS was used to provide discoidal morphology. Retention of the valley and broad bilayer peaks indicated that samples had retained their structures.*

Cytotoxicity Assay of the ND

To characterize the nanodisc formulation in the biological system in in-vitro conditions, it was necessary to screen the formulation for cytotoxicity and ensure that it would not induce significant cytotoxicity to microglial (HMC-3) and neuronal (SH-SY5Y) cells. Since our

formulation was developed to target the brain, it was essential to observe the effect of ND on these cells for any neurotoxicity or cytotoxicity. A cell viability (MTS) study was performed for both 1:20 and 1:4 NDs as per the manufacturer's instruction (G3582, Promega, Madison, WI, USA). NDs were introduced to these cells separately at varying TFV drug concentrations of 0.01-0.1 mg/mL and incubated for 72 hours.

Overall, cell viability results indicated that ND was less toxic to HMC-3 cells than SH-SY5Y cells. The 1:20 ND formulation was found to be significantly toxic at concentrations above 0.075 mg/mL for HMC-3 cells (Figure 7). For SH-SY5Y cells, 1:20 ND was found to be only statistically significant at 0.1 mg/mL but is observed to have a decrease cell viability starting at 0.05 mg/mL. 1:4 ND formulation was significantly toxic at concentrations above 0.05 mg/mL for SH-SY5Y cells. FD-TFV was not considered to be significantly toxic when compared to the control. A separate setup to evaluate the effect of empty NDs was done as well, where HMC-3 and SH-SY5Y cells were treated with varying lipid concentrations of the bicellar ND which associate with the TFV concentrations used prior (Table 3). Results showed that lipid concentrations above 0.08% and 0.05% were considered significantly cytotoxic for HMC-3 cells and SH-SY5Y cells, respectively (Figure 8). This indicated that at higher drug concentrations associated with higher lipid concentrations, there is an observed decrease in cell viability.

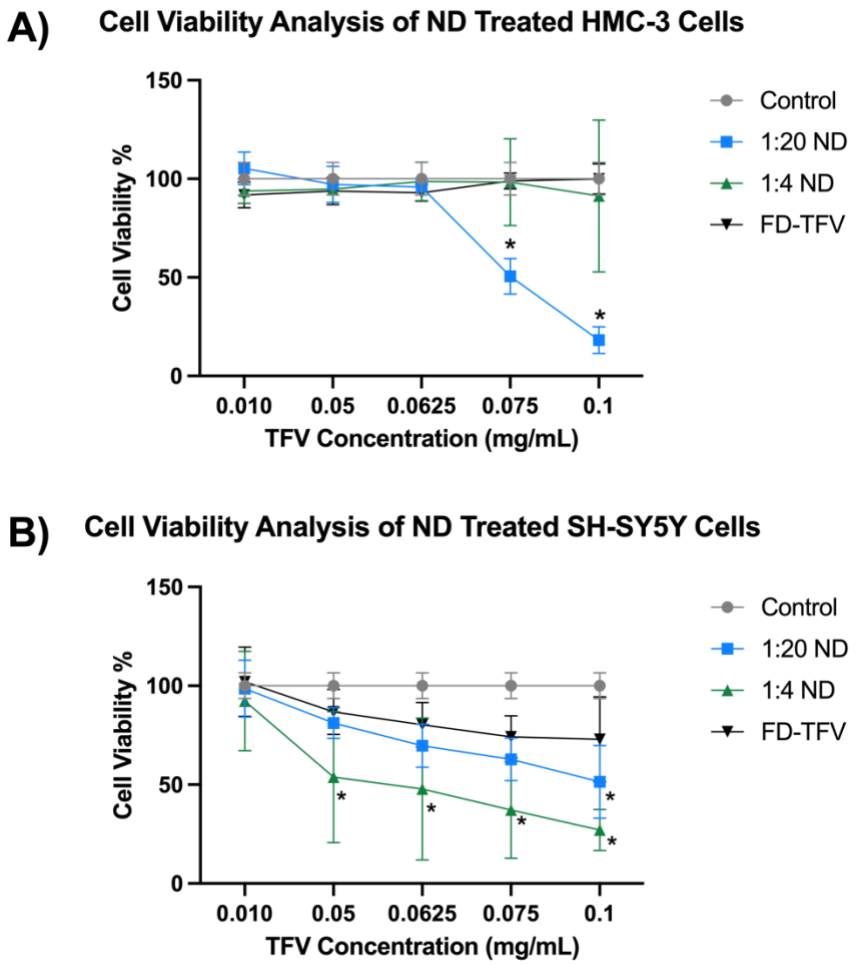

Figure 7: Cell viability assay of ND on HMC-3 and SH-SY5Y cells*; A cell viability analysis of A) HMC-3 and B) SH-SY5Y cells when treated with ND at a drug-to-lipid ratios of 1:20, 1:4 and FD-TFV Graphical representation of was made as cell viability percentage (%) at different TFV concentrations (0.01 mg/mL – 0.1 mg/mL) of the formulations. Untreated (control) cells were considered 100% viability and % cell survival was monitored based on control. Cell viability % was measured as mean ± SD of three independently replicated experiments. Statistical significance was calculated by two-way ANOVA test with posthoc Dunnett's multiple comparisons test. A value of $p < 0.05$ was indicative of significance compared to the control (*).*

Table 3: Drug-to-lipid lipid concentration at associated drug concentrations.

TFV Concentration (mg/mL)	Lipid Concentration (%)	
	1:4 ND	1:20 ND
0.01	0.01	0.05
0.05	0.05	0.26
0.0625	0.066	0.33
0.075	0.08	0.4
0.1	0.1	0.53

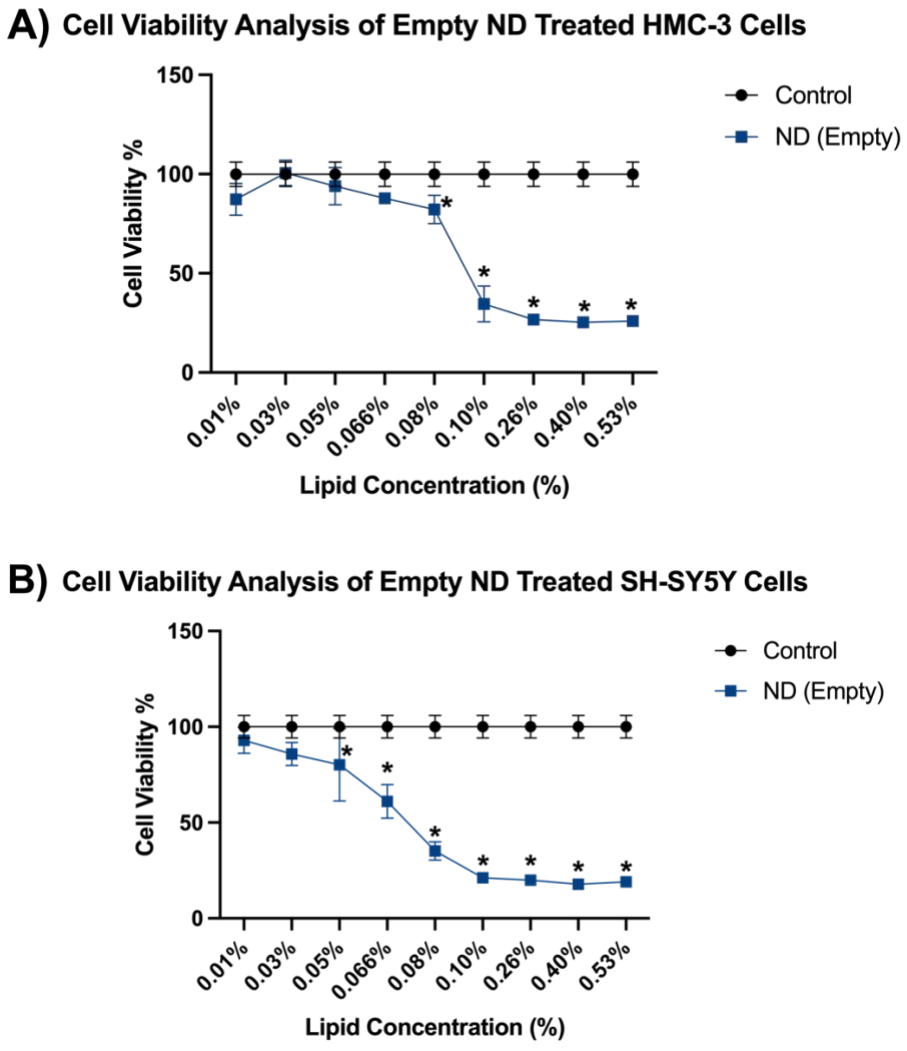

Figure 8: Cell viability assay of empty ND on HMC-3 and SH-SY5Y cells*; Graphical representation was made as cell viability percentage (%) varying lipid concentrations of the ND*

(0.01-0.53%). Untreated (control) cells were considered 100% viability, and % cell survival was monitored based on control. Cell viability % was measured as mean ± SD of three independently replicated experiments. Statistical significance was calculated by one-way ANOVA test with posthoc Dunnett's multiple comparisons test. A value of $p < 0.05$ was indicative of significance compared to the control (*).

ROS Production by ND on HMC-3 and SH-SY5Y Cells

While nanomaterials possess unique properties that have increased their use, understanding their interactions within biological systems is important to note. As a first approach to predict the inflammatory response on neuronal cells, the ROS production of HMC-3 and SH-SY5Y cells was evaluated. HMC-3 (Figure 9A) and SH-SY5Y cells (Figure 9B) were treated with the different drug-to-lipid ratios of 1:20 and 1:4 at varying TFV drug concentrations (0.01 – 0.1 mg/mL). A negative control antioxidant (catalase) and positive control (H_2O_2) were used on non-treated cells. A simultaneous setup was also performed for empty NDs at varying lipid concentrations. Since a significant drop and then a plateau in cell viability was seen for lipid concentration above 0.1%, ROS assay was only done for lipid concentrations of 0.01%-0.1% to observe ROS production (Figure 10).

Both HMC-3 cells and SH-SY5Y cells undergoing the treatment of 1:20 ND were shown to significantly increase ROS production at all of the tested concentrations (0.01 – 0.1 mg/mL) compared to the control (Figure 9). SH-SY5Y cells were undergoing the treatment of 1:4 ND did not show a significant increase in ROS production at tested concentrations up to 0.1 mg/mL for both cell lines.

We also analyzed the FD-TFV's effect on ROS production of HMC-3 and SH-SY5Y cells. For both cell lines, the FD-TFV did not induce a significant increase in ROS production, indicating that the FD-TFV does not actively cause inflammatory properties at the tested concentrations. Overall, these results indicated that ROS production in 1:4 ND treated cells was closer to untreated cells, suggesting this formulation’s potential for further optimization.

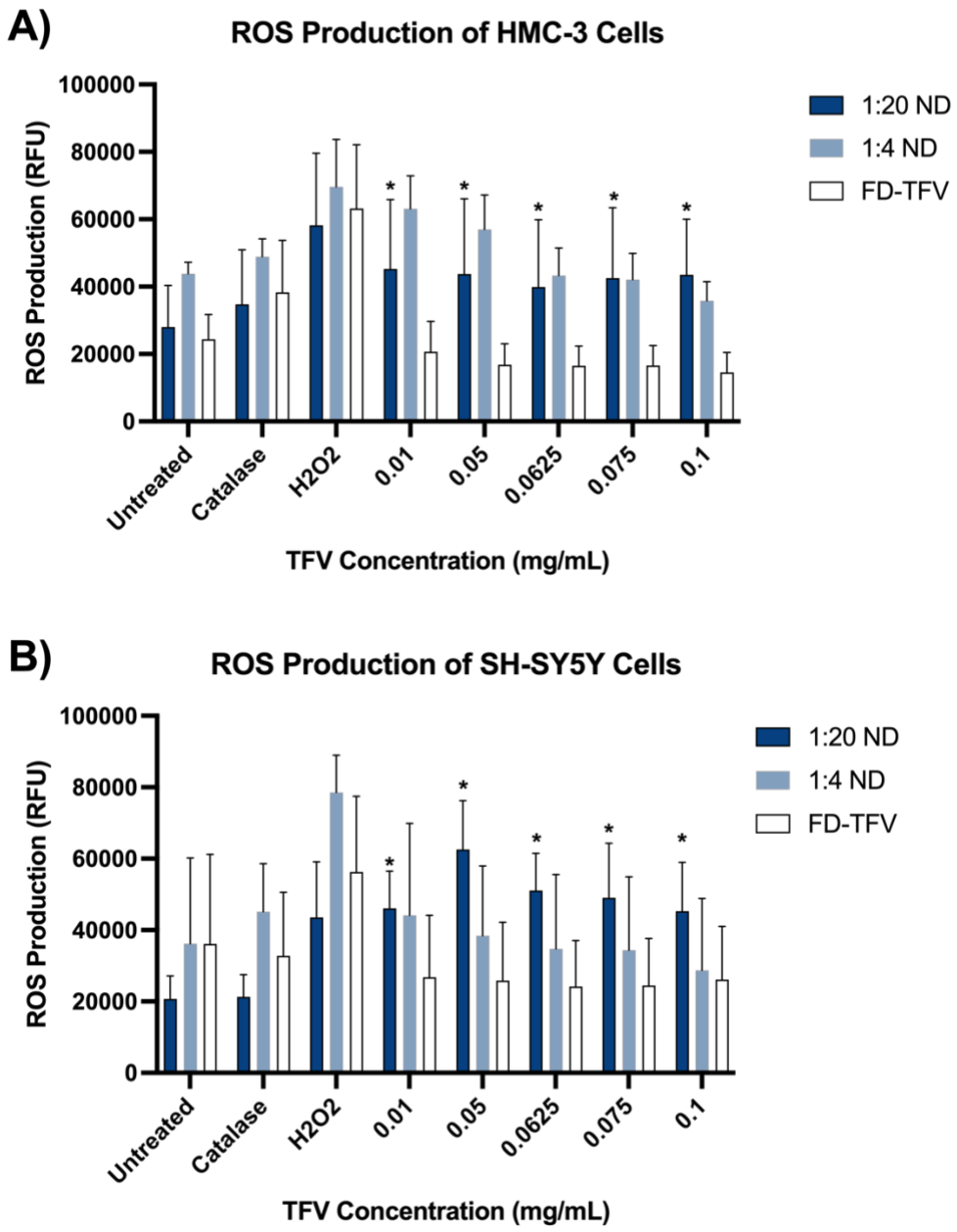

Figure 9: Effect of ND at 1:20 and 1:4 and FD-TFV on ROS production on HMC-3 and SH-SY5Y cells; *A) HMC-3 and B) SH-SY5Y cells were exposed at different concentrations (0.01 mg/mL – 0.1 mg/mL). Graphical representation was made in ROS production; ROS production was measured in terms as mean ± SD relative fluorescence units (RFU) of three independently replicated experiments. Statistical significance was calculated by two-way ANOVA test with*

posthoc Dunnett's multiple comparisons test. A value of $p < 0.05$ was indicative of significance compared to untreated cells (*).

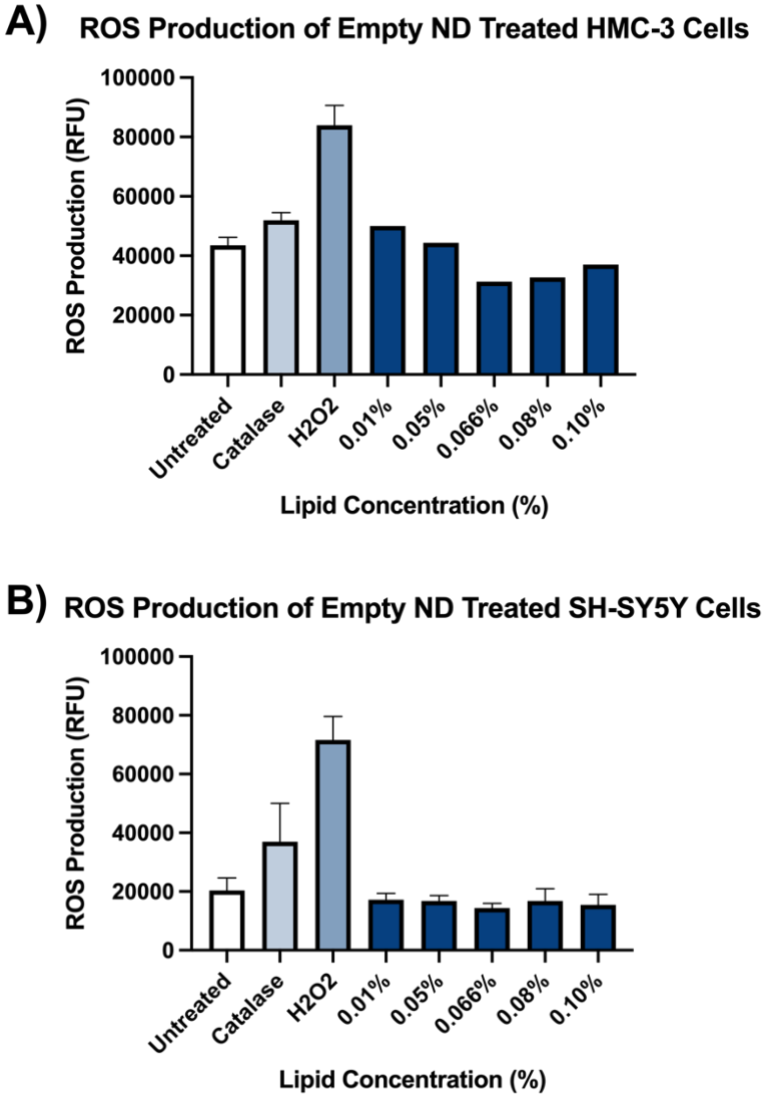

Figure 10: Effect of empty ND on ROS production on HMC-3 and SH-SY5Y cells; *HMC-3 and B) SH-SY5Y cells were exposed at different lipid concentrations (0.01-0.1%). Graphical representation was made in ROS production; ROS production was measured in terms of mean ± SD relative fluorescence units (RFU) of three independently replicated experiments. Statistical significance was calculated by one-way ANOVA test with posthoc Dunnett's multiple*

comparisons test. A value of $p < 0.05$ was indicative of significance compared to untreated cells (*).

In-Vitro Sustained Drug Release Assay

The nanodisc formulation's extended drug release profile was determined in phosphate buffer saline (PBS) using an equilibrium dialysis system. The released TFV from the dialysis bag into the outside environment was sampled at different time points up to 14 days and was measured by LC-MS/MS. The dialysis bag used in these experiments was selected for its pore size of 6-8 kDa MWCO. Our nanodisc typically has an average molecular weight of 3.7 kDa without drug, so the selection of 6-8 kDa MWCO was selected so that drug transport would not be a limiting factor. Simultaneously, a separate set up with the same concentration and volume of FD-TFV was used as a control. Results were expressed as the percentage of total TFV released into the system compared to the initial concentration. It was observed that 63% of FD-TFV was release within 4 hours. Compared to FD-TFV, the 1:4 ND showed 35% drug release within 4 hours (Figure 11). Compared to the FD-TFV, the 1:20 ND showed 0.18% drug release within 4 hours and showed a significant, sustained drug release of TFV, *in-vitro* condition. (Figure 11).

Overall, when comparing both 1:20 ND, 1:4 ND, the FD-TFV had a significantly faster TFV release, although it is considered delayed in terms of free drug. However, between 1:20 ND and 1:4 ND, 1:20 was shown to have a significantly extended release than 1:4 ND (Figure 11).

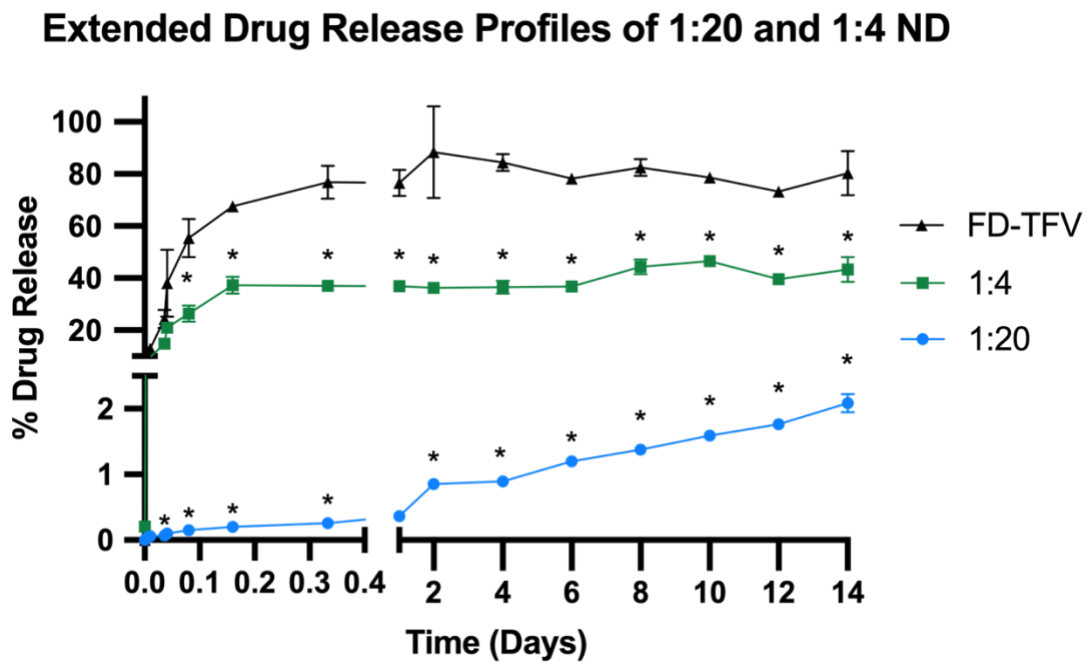

***Figure 11: Drug release profiles of ND (1:20 and 1:4) vs. FD-TFV* in-vitro**; *Graphical representation was made in terms of cumulative drug release percentage (%) and was measured in terms as mean % ± SD of n = 3. Statistical significance was calculated by two-way ANOVA test with posthoc Dunnett's multiple comparisons test. A value of $p < 0.05$ was indicative of significance when compared to FD-TFV (*). Note: Some initial timepoints are not marked for significance due to overlapping in graph.*

Drug Release *In-Vitro* Environment through the BBB

The ND was further investigated for its drug delivery property crossing the BBB. An *in-vitro* BBB model was set up to mimic the biological barrier encountered in drug delivery towards HIV-1 residing in the brain and understand the drug release kinetics of the ND in the BBB environment. In this experiment, an *in-vitro* BBB model was set up as explained in the method section. The BBB model's integrity was characterized by measuring the TEER values before and

after the ND exposure. The range of TEER values was from 130 to 150 Ω at the beginning and the end of the experiments (Figure 12A). The range of TEER values was similar to all three groups including the control, ND and FD-TFV groups. The TEER values indicated the consistent integrity of BBB throughout the experiment, confirming the contribution of BBB in transporting the ND formulation from the apical to basolateral side of BBB. The percentage of drug release of TFV from 1:4 ND formulation was compared with the FD-TFV and the pattern indicated that the 1:4 ND has a sustained release up to four days, which was not significantly different from FD-TFV (Figure 12B).

Based on the results of this *in-vitro* BBB model, 1:4 ND was observed to have similar drug release characteristics when compared to FD-TFV. In contrast, 1:20 ND formulation was shown to have extended -release properties and was found to be significantly different from that of the FD-TFV. These results are similar to those seen in the dissolution study (Figure 11).

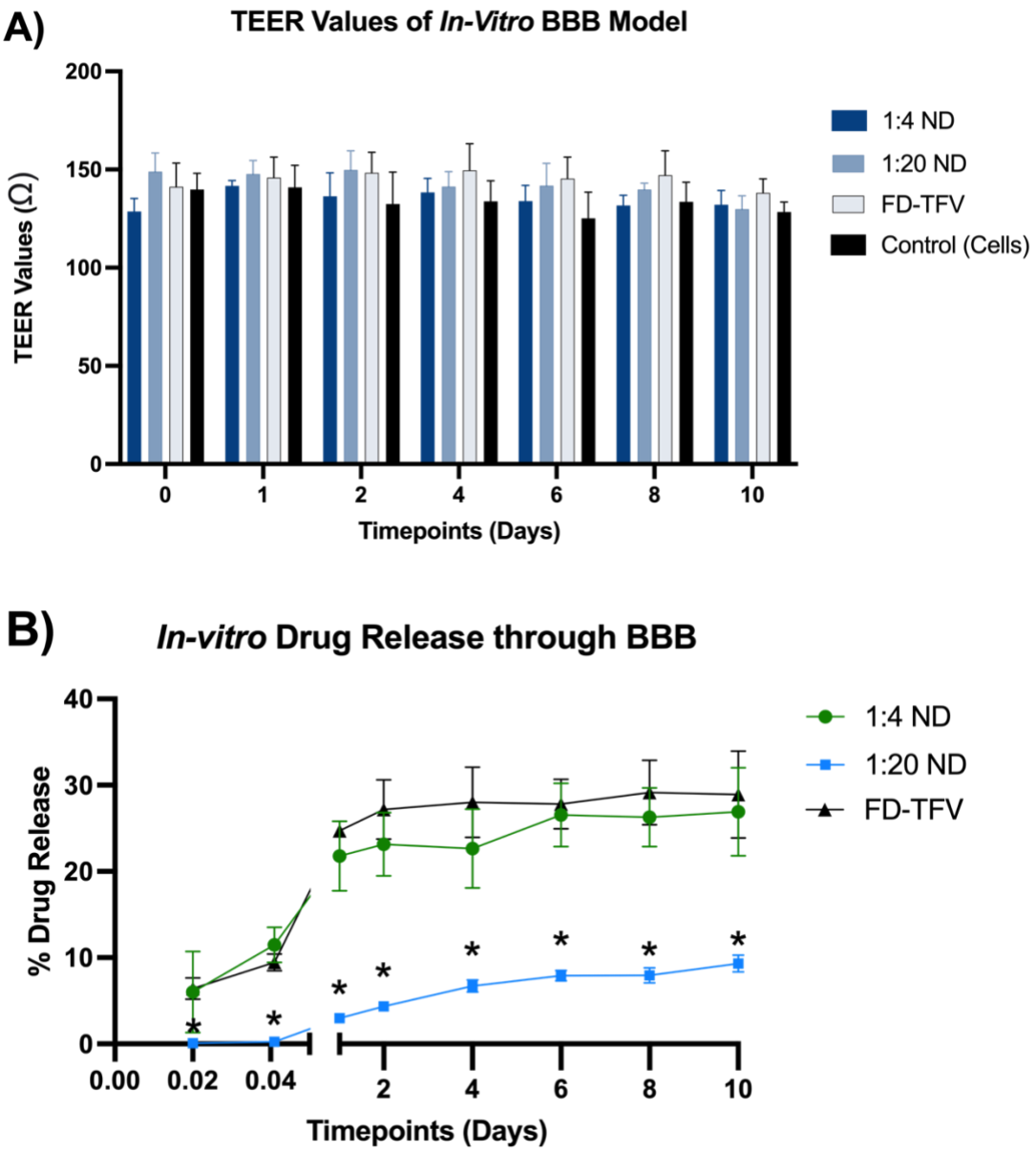

Figure 12: BBB model's TEER values and sustained drug release study from 1:20 and 1:4 ND* in-vitro; 1:20 ND, 1:4 ND and FD-TFV were introduced into the apical chamber of the BBB model. A) TEER values of the BBB were measured to ensure formulations did not significantly affect the integrity of the BBB. B) Drug release of formulations through the BBB was observed and measured up to 10 days. Graphical representation was made in terms of average drug release percentage (%) and was measured in terms as mean % ± SD of n = 3. Statistical*

significance was calculated by two-way ANOVA test with posthoc Dunnett's multiple comparisons test. A value of $p < 0.05$ was indicative of significance when compared to FD-TFV (*).

Cell Uptake and Characterization of Extended-Release from ND

To evaluate the intracellular uptake of TFV in microglial cells, and *in-vitro* cellular uptake study was performed. We evaluated the cellular uptake of our two formulations (1:20 ND and 1:4 ND) and FD-TFV as a control, simultaneously and monitored the uptake and release of TFV over 24 hours. Our results showed different uptake within our formulations. Maximum uptake was observed at 1 hour for 1:20 ND, 2 hours for 1:4 ND, and 2 hours for FD before trending down (Figure 13). Looking at the physiochemical characteristics of TFV, this drug won't cross the cell membrane of microglial cells easily. This is observed in the cell uptake experiment. The concentrations measured within the samples were found to be below or around the limit of quantification which leads us to understand that only a small amount of TFV can cross the cell membrane. This small window of cellular uptake could indicate that there is a certain capacity that microglia cells can uptake TFV, or there could be the formulations physical characterization preventing a higher uptake of the ND.

Observed results from this cellular uptake study indicated that 1:4 ND is observed to accumulate tenofovir within the cell better than 1:20 ND and FD-TFV formulations. However, the short windows of drug uptake by the microglial cells could indicate that the size and surface charge of the ND could be a contributing factor.

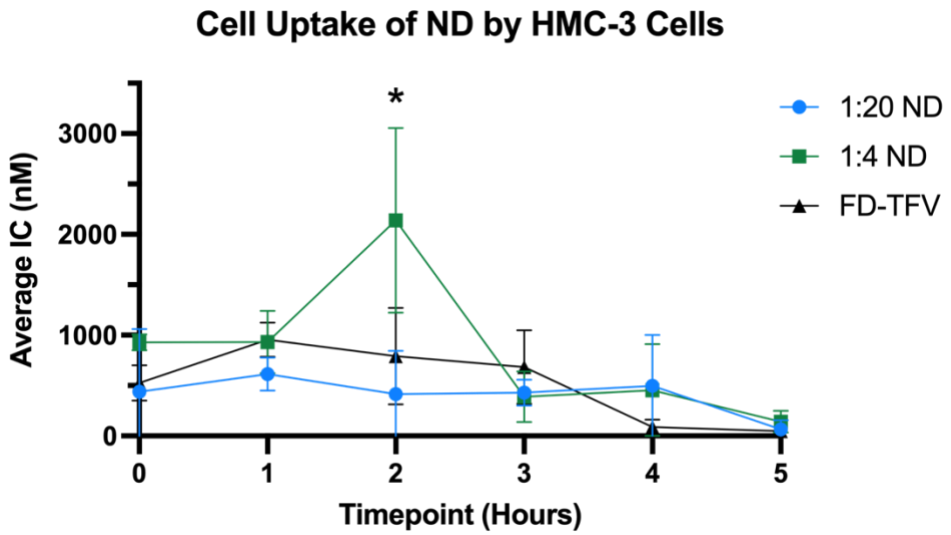

Figure 13: **In-vitro *cellular uptake study of ND (1:4 and 1:20) and FD-TFV***; *Graphical representation was made in terms of average intracellular concentration (IC) and was measured in terms as mean ± SD of n = 3. Statistical significance was calculated by two-way ANOVA test with posthoc Dunnett's multiple comparisons test. A value of p < 0.05 was indicative of significance when compared to FD-TFV (*).*

In-Vivo Maximum Tolerated Dose Study and Pharmacokinetic Analysis of ND

During the MTD study, Male and female BALB/c mice were treated with a single iv dose administration at 0, 2, 10, 15, or 20 mg/kg. Mice were observed at pre-determined timepoints, appeared normal throughout the phase, and tolerated the ND's varying concentrations well. The highest MTD dose level of TFV was selected at 20 mg/kg to continue with the PK study.

During the PK study, male and female BALB/c mice were administered a single dose iv administration at 20 mg/kg TFV in ND formulation (Group 6) and unformulated (FD-TFV) tenofovir in sterile saline formulation (Group 7). PK data analysis was performed using the plasma concentrations of TFV in the mice (Figure 14). Plasma samples were collected for up to

48 hrs and 72 hours. The plasma concentration of ND formulation were 44,300 ng/ml (males) and 34,400 ng/ml (females), and for FD-TFV (Group 7) were 46,000 ng/ml (males) and 79,300 ng/ml (females) (Table 4). Statistical analysis indicated significance amongst FD-TFV treated females, this may due to individual animal variation as one mouse had plasma concentrations about 2-fold higher at the first time point than the other females within the group. Exposure based on area under the plasma concentration curve to the last time point (AUC_{last}) values for the lipid formulation was 8,710 ± 195 hr•ng/ml and 7,590 ± 686 hr•ng/ml for males and females, respectively. In the mice receiving TFV in a sterile saline formulation, the area under the plasma concentration curve to the last time point (AUC_{last}) values was higher, 9,870 ±697 hr•ng/ml (males) and 15,200 ± 1,680 hr•ng/ml (females). The AUC_{inf} values were higher in unformulated TFV (Group 7) than ND formulation (Group 8).

Table 4: Effect of ND and FD-TFV on PK in Male and Female BALB/c Mice after IV Administration, 20 mg/kg

Group	Sex	$t_{1/2}$ (hr)	C_0 (ng/mL)	AUC_{last} (hr•ng/ml)	Cl (mL/hr/kg)	Vz (mL/kg)
ND	M	4.9	44,300	8,710	8,750	16,300
ND	F	5.2	34,400	7,590	7,630	19,800
FD-TFV	M	5.3	46,000	9,870	9,930	15,500
FD-TFV	F	5.3	79,300	15,200	15,300	9,930

The clearance (Cl) values for Group 6 were higher than the Cl values observed for Group 7. The volume of distribution (Vz) was high for all groups with values greater than 10 mL/kg; this result is consistent with a drug accumulating intracellularly, such as TFV [63]. The terminal

$t_{1/2}$ was 4.9 hr and 5.2 hr for Group 6 males and females, respectively. For Group 7, the terminal $t_{1/2}$ was 5.3 hr for both sexes.

Overall, some differences in the PK of TFV when administered encapsulated in ND compared to FD-TFV. In male mice, the PK parameters varied slightly between the two formulations, with AUC values about 10% higher for FD-TFV. Administration of TFV as FD-TFV in female mice resulted in plasma exposure that was 2 fold higher base on mean value of C_0, AUC_{last} and AUC_{inf} while Cl and Vz values were lower.

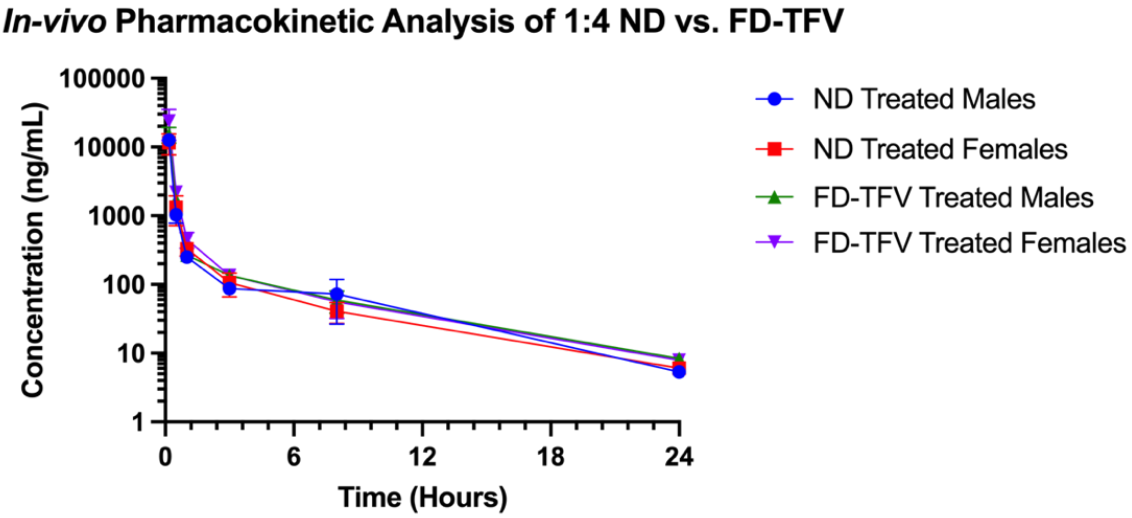

Figure 14: Plasma concentrations of TFV after a single iv dose to male and female BALB/c mice*; Graphical representation was made in terms of plasma concentration (ng/mL). each data point represents the mean ± SD of n = 12 mice. FD-TFV treated females were found to be statistically significant compared to other treatment groups; however, this may due to an individual animal variation as one mouse had a higher plasma concentration at first time point than other mice in group. Statistical significance was calculated by two-way ANOVA test with posthoc Dunnett's multiple comparisons test. A value of $p < 0.05$ was indicative of significance.*

In-Vitro Sustained Drug Release Assay of Liposomal Structure

NDs were initially used based on their superiority in having a greater cellular uptake than their spherical counterparts in addition to their small size that would allow them to bypass the BBB to treat HIV-1. However based on our *in-vitro* and *in-vivo* characterizations of the ND formulation, it was decided to adjust our formulation to form a liposomal structure instead of a bicellar ND structure to achieve better pharmacokinetics of the formulation. Liposomes are similar to the ND formulation as they are made up of the same molecular weight, chemical composition, lipid concentration, appearance and pH as the ND (Table 5). Liposomes have a better capability to encapsulate TFV within its structure due to its aqueous core which will then have much slower release of the drug.

Table 5: Comparison Table of ND vs. Liposomal Structure

Test	**Nanodisc**	**Liposome**
Molecular Weight	760	760
Size (Hydrodynamic Radius)	~7.5-13 nm	~400 nm
Drug-to-Lipid Ratios	1:4 1:20	1:2.3 1:3.7
Shape	Discoidal 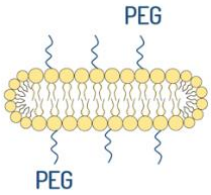	Spherical 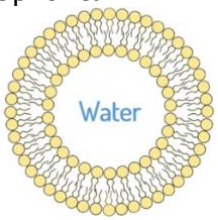
Active Pharmaceutical Ingredient (API)	DPPC, DSPE-PEG, DHPC, DPPG	DPPC, DPPG

pH	6.4	6.4
Lipid Concentration	5%	5%
Appearances	Clear, colorless	Clear, colorless
Stability	1 week at 4°C	1 week at 4°C
Storage Conditions	At room temperature (25°C)	At room temperature (25°C)

In order to study the liposome formulation's extended drug release kinetics, a drug release study was done in PBS using an equilibrium dialysis system. Three versions of the liposome-TFV were synthesized at varying drug-to-lipid ratios: liposome 1 (1:2.3), liposome 2 (1:3.7) and liposome 3 (1:3.7) (Table 5). Liposomes 2 and 3 have the same drug-to-lipid ratios but different lipid charge densities of 2% and 5%, respectively. Liposome 1 has a lipid charge density of 5%. The released TFV from the dialysis bag into the outside environment was sampled at different time points up to 14 days and was measured by a NanoDrop Microvolume Spectrophotometer. Simultaneously, a separate setup with the same concentration and volume of FD-TFV was used as a control. Results were expressed as the cumulative total of TFV released into the system compared to the initial concentration (Figure 15). It was observed that 100% of the FD-TFV was released within 4 hours; whereas Liposomes 1, 2, and 3 showed a 56-57% drug release of TFV within 4 hours. This indicates the liposomal formulations have a sustained drug release up to 4 days when compared to FD-TFV. FD-TFV was observed to have a significantly faster drug release than the liposomes; however, it was observed to trend downward for the later timepoints of the experiment. This downward trend may be caused by byproducts from the FD-TFV in the external environment.

Overall, results from this *in-vitro* drug release study indicated that the liposome formulations could have a more sustained drug release compared to FD-TFV. In comparison to

liposomes, 1:20 ND does show better sustained release properties; however, our characterizations of the formulation showed that it would not be a suitable fit to continue forward for a TFV encapsulation.

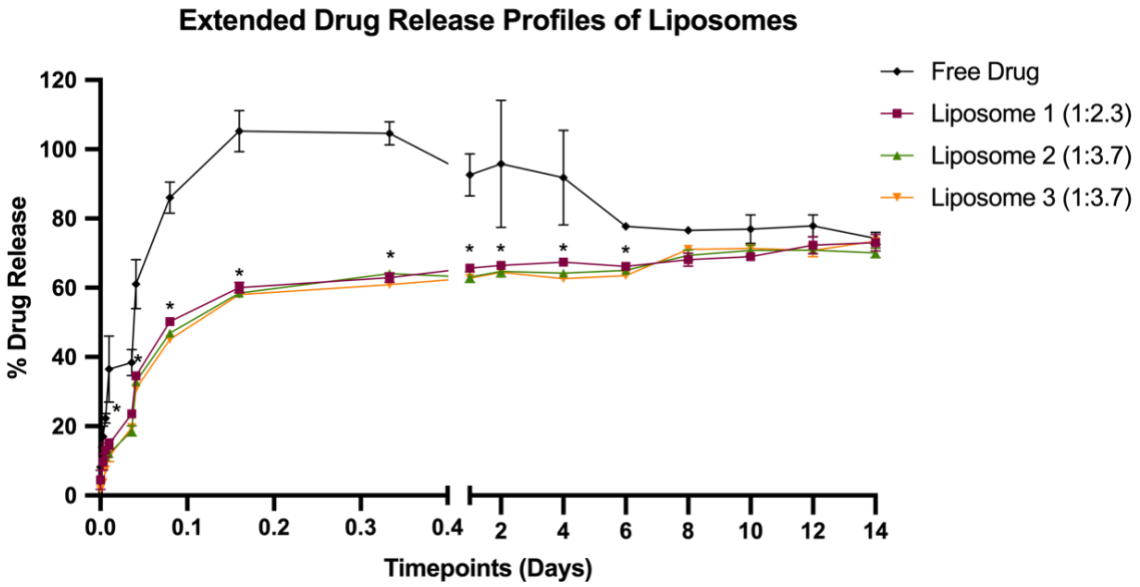

Figure 15: Extended drug release profiles of liposome-TFV at varying drug-to-lipid concentrations*; Liposomes had following drug-to-lipid ratios: Liposome 1 (1:2.3), Liposome 2 (1:3.7) and Liposome 3 (1:3.7). Graphical representation was made in terms of cumulative drug release percentage (%) and was measured in terms of mean % ± SD. Statistical significance was calculated by two-way ANOVA test with posthoc Dunn's test. A value of $p < 0.05$ was indicative of significance (*). Liposomes 1, 2 and 3 had statistically significant drug release up to 6 days compared to FD-TFV.*

CHAPTER IV

DISCUSSION

Designing and developing long-acting and sustained-release drug formulation that can deliver antiretroviral drugs towards the brain is still a current challenge in HIV-1 infection treatment. Even though multiple approaches have been taken to bridge the gap, the research is still ongoing to find an ideal formulation that can provide a long-term inhibition of the virus from the viral reservoir like the brain. In this regard, the nanocarriers, such as nanodisc and liposomes, have significant potential to bring a new nanoformulation to provide a solution. We hypothesized in this study that a nanodisc-based delivery of TFV would be safe and effectively perform extended release which will help in HIV-1 treatment to the brain.

NDs are composed of phospholipid mixtures of long-chain lipids, dipalmitoyl phosphocholine (DPPC), and short-chain lipids, dihexanoyl phosphocholine (DHPC). They have many advantages, such as attainable high lipid concentration, uniform size, robust formation, and easy integration of hydrophobic/hydrophilic molecules, allowing them to be used as nanocarriers [64]. Recent studies have established that the nanodisc is a low-polydispersity, spontaneously-forming discoidal shape with a diameter of about ~30 nm and a thickness of ~5 nm and has shown an increased cellular uptake when compared to spherical vesicles of the same chemical composition. [31]. Therefore, the nanodisc represents an attractive drug delivery system to have great potential to serve as delivery nanocarriers to bypass the blood-brain barrier to assist in inhibiting HIV-1 replication within the brain.

This study focused on the encapsulation of the anti-HIV drug TFV into the nanodisc. TFV is a nucleoside reverse transcriptase inhibitor used in combination with other anti-HIV drugs in the cART regimen [16, 49]. Currently, TFV is one of the most commonly recommended anti-HIV drugs recommended by WHO and the US Department of Health and Human Services (HHS) [65, 66]. MEP and MSLP provided insights into the molecular structure, lipophilicity, and surface charge of TFV and characterized TFV interactions within its entrapment of the ND (Figure 4). MEP and MLSP showed TFV as an extremely lipophobic molecule that can limit the drug's incorporation within the bicellar core; however, the nanodisc can entrap both hydrophilic and lipophilic molecules due to the amphiphilic nature of the phospholipids [67, 68]. DLS was used to investigate the size of the drug loaded-NDs, and the results of the DLS confirmed the uniformity of the nanodiscs for individual TFV-ND samples (Figure 5).

SAXS provided insights into the discoidal morphology of the ND. By simulating the proposed ND structures' electron density profile, SAXS probes the average arrangement of molecules in NDs. In a well-defined ND, the SAXS data generally contains a series of peaks for $q > 0.07$ Å^{-1}, which correlate to the lipid bilayer structure (Figure 6). The retention of the valley and broad bilayer peak in the SAXS patterns of the drug-loaded NDs in both 1:4 and 1:20 samples indicates that the NDs maintained their structures. However, the SAXS data indicated the role of TFV's chemical structure and its influence on NDs' internal structure. The overall diameter of the NDs increases with higher drug content, R_{core} remains practically constant for TFV-NDs. Current results seem consistent with the recent study that short-chain DHPC with large spontaneous curvature, mixed with DPPC, induces defects on the DPPC bilayer, thus making the membrane more actively interact with foreign hydrophobic species [56]. The R_{core} suggests that TFV mainly resides at the face (closer to the surface and polar water environment)

even with increased TFV composition judging by the invariance of R_{core}. Therefore, the ND formulation was prepared at the different drug to lipid ratios (1:4 to 1:20). This drug to lipid ratio was optimized based on the drug encapsulating capacity at the core of the ND. The amount of bicellar lipid had significantly contributed to the drug loading capacity of the ND formulation. Therefore, formulations with the lowest (1:4) and highest (1:20) lipid concentrations were selected for further study. The difference in 1:4 and 1:20 drug-to-lipid ratios is the amount of lipid content within the ND's bicelle; however, the amount of drug concentration for both remains the same. This observation also indicated the contribution of DPPC and DHPC in this process of biceller assembly.

To evaluate ND in a biological system, it was essential to screen the nanoformulation for cytotoxicity on ND -treated microglial and neuronal cells. cell viability (MTS) study was performed for 1:20 ND, 1:4 ND and FD-TFV on HMC-3 and SH-SY5Y cells at varying concentrations of 0.01-0.1 mg/mL (Figure 7). A separate setup for the treatment of empty NDs on cells was also evaluated to access if the lipid formulation (Figure 8). MTS results indicated that 1:20 ND was seen to cause a decrease in cell viability for HMC-3 and SH-SY5Y cells at higher TFV concentrations which are associated with higher lipid content (Table 3). These results can also be observed it cell viability analysis of empty NDs where lipid concentrations were found to have significant decrease at 0.08% and 0.05% for HMC-3 and SH-SY5Y cells, respectively. While statistically, the decrease in cell viability from 1:20 ND in SH-SY5Y cells was only significant at 0.1 mg/mL, there is still a decrease in cell viability starting at 0.05 mg/mL. While lipid-based formulations are safe, biocompatible and display low toxicity, there is still a level of concern for high lipid concentrations which are seen within this study and the study of ND's toxicity towards neuronal cells remains limited [69]. One report also has proposed

that surface coating, such as added PEGylation or PGLA, induces the toxicity of polymeric NPs towards human macrophages [70, 71]. Results also indicated that SH-SY5Y cells were more susceptible to toxicity than HMC-3 cells as both formulations (1:4 and 1:20) were observed to cause a decrease in cell viability. Considering MTS results, 0.0625 mg/mL was selected for further study even though this concentration was relatively toxic to SH-SY5Y cells. This is because microglia will be hosting the drug for a longer period in the brain as the HIV-1 reservoirs and perform sustained release of ND, whereas neurons will have secondary exposure of the ND. Therefore, based on previous publications [42, 72] and our current analysis the concentration was selected.

The ND was further evaluated to observe if the formulations caused increased ROS production and oxidative stress to a cellular environment after treatment as neuronal cells are susceptible to ROS [73]. This characterization is fundamental as nanoparticles can trigger ROS production and oxidative stress, leading to nanoparticle induced neurotoxicity. Therefore, a cell inflammatory analysis (ROS) assay is important to be undertake in order to limit these problems before it goes for *in-vivo* characterization and clinical trials [35]. A ROS assay was performed for 1:20 ND, 1:4 ND and FD-TFV on HMC-3 and SH-SY5Y cells at TFV concentrations 0.01 – 0.1 mg/mL (Figure 9). The ROS assay analysis had shown that 1:20 ND induced a significant increase in ROS production for both HMC3 and SH-SY5Y cells. ROS production in 1:4 ND treated cells was closer to both untreated cells in both cell lines, indicating this formulation's potential for further optimization.

Additionally, FD-TFV treated cells did not induce ROS production in the cell lines (Figure 10). This suggests that it may be the ND combination, at high lipid concentrations, with TFV that induces the ROS production in these cells. The observation of induced ROS production

from 1:20 can be due to several multiple factors regarding the ND composition. Critical chemical and physical determinants that have been found to affect the generation of ROS include: molecular size, shape, oxidations status, solubility and degree of aggregation [74]. The production of ROS from a particular nanomaterial is dependent on the physical and chemical composition of the nanomaterials, as well as the tested cell types [74]. It has also been suggested that nanoparticles with smaller particles sizes, such as the ND, are reported to induce a higher ROS due to having a high surface-to-volume ratio and high surface charge [75]. Particle size of a nanoparticle determines the number of reactive groups/sites on the nanoparticle surface [75]. Overall, the optimization of the ND is dependent on several other factors, such as long-term stability, sustained release and therapeutic efficacy. Considering the results from the ROS assay, both 1:20 and 1:4 NDs were further evaluated for *in-vitro* BBB model (Figure 12) and cellular uptake study (Figure 13) at the concentration of 0.0625 mg/ml to understand the drug release properties of the formulations.

The drug release behavior of a nanoformulation is an important factor as its directly related to drug stability and therapeutic results and the overall formulation development for the stability and sustainability of the drug formulation in a biological environment, such as the human body [76]. To observe the drug release profile of 1:20 and 1:4 ND formulations, they were further characterized by a dissolution study (Figure 11). The 1:20 nanoformulation demonstrated a significantly sustained formulation compared to FD-TFV and 1:4 ND. It should be noted that during LC-MS/MS analysis of 1:20 NDs drug release profile there was a detection of a prodrug-like molecule of TDF, although our formulation was not made with the prodrug TDF. This may due to byproducts or metabolites found from TFV in the 1:20 sample that may have been identified as structurally similar as TDF [77, 78]. A loss of TFV into byproducts has

been previously attributed to pH which may have played a likely factor in the 1:20 sample [79]. Additionally, it is essential to note that there was no other detection of prodrug in 1:4 ND and FD-TFV samples.

The release profile of FD-TFV showed a limitation in the release across the dialysis membrane, which could be attributed to the retardation effect of the tight composition in cellulose structure [80, 81]. Drug release observations of the NDs further assured that the formulation with higher lipid content is more stable in biological buffer conditions (PBS with 0.1% Tween 20). Considering the structure of the hydrophilic formulation on the surface and hydrophobic inside, results suggest that more lipids within the bicelle are required to hold the drug within the formulation [82]. Lipid content of a nanostructure helps govern the drug loading capacity, prolonged action and the overall stability of the formulation which suggest why 1:20 ND may have better encapsulation compared to 1:4 ND [82]. In addition, since the formulation has an automatic encapsulation property without any experimental procedure, the amount of the drug it will also hold largely depends on how well the ND is formed with a particular concentration of lipids [50, 82]. Overall, the drug release study had established that 1:20 ND were significantly more stable than 1:4 ND that could translate into having better pharmacokinetics *in-vivo.*

This formulation was further evaluated into an *in-vitro* BBB model environment to observe its efficacy to cross the BBB and deliver TFV to the cells (Figure 12). *In-vitro* BBB models are essential in developing improved therapeutics for the treatment of neurological disorders [83]. It has been observed that like many other antiretroviral drugs, TFV also has a limited penetrance through the CNS [84], therefore it is important to know if the current formulation has an improved drug delivery capacity across the BBB. In the *in-vitro* BBB model,

it was important to observe that exposure to ND or FD-TFV would not compromise the BBB integrity throughout the experiment which was not impacted (Figure 12A). Figure 12B indicated that drug release from the apical to the basolateral chamber of the BBB model by the formulations. The study showed sustained drug release properties of 1:4 ND up to four days, similar to the results overserved in the ND in the dissolution study via dialysis bag (Figure 11). In this regard, 1:4 ND was observed to have similar drug release characteristics when compared to FD-TFV. Whereas, 1:20 ND formulation was shown to have extended release properties and was found to be significantly different from that of the FD-TFV. As previous studies have established that drug transport across the BBB largely depends on the phagocytic property of HBMVEC cells on the BBB, macrophage mediated drug delivery, and the contribution of biological transporters present on the BBB [85]. Therefore, the properties of the drug and ND formulation along with the above mentioned factors could affect the overall drug formulation transport across the BBB. It is noteworthy that the drug release of the FD-TFV and NDs across the BBB is regulated by the biological transporters that are present on both sides of the BBB [86]. Often times it was observed the drug release capacity across the BBB might be higher; however, those formulations struggle with sustained release properties as indicated in our observation. Even though FD-TFV and 1:4 ND could cross the BBB efficiently, it did not have a sustained release property such as the 1:20 ND formulation.

These formulations were also evaluated for their microglial uptake via an *in-vitro* cell uptake study. Microglia are considered the major reservoir of HIV-1. They are the main host of the ND upon delivery to the brain; therefore, the cell uptake capacity of the HMC-3 cells was important to observe. This observation would help in determining the drug retention capacity of the brain. Results showed a maximum TFV uptake observed at 1 hour for 1:20 ND, 1 hour for

FD-TFV and 2 hours for 1:4 ND. The short windows of drug uptake by the microglial cells could indicate that the size and surface charge of the ND is a contributing factor. Previous studies have shown that for cellular uptake of nanoparticles (NP), there was an optimum size of 50 nm; they are internalized more efficiently and at a higher uptake rate [87]. Whereas smaller NPs (15-30 nm), uptake was shown to decrease and enter cells less effectivity since these particles can go in and out of cells more easily [87, 88]. The PEGylation of the current formulations could also be contributing to the decrease cellular uptake as it was found that PEGylation reduced a study's nanoparticle uptake and delayed the rate of NPs uptake when compare to non-PEGylated nanoparticles [85].

Based on the *in*-vitro studies, an *in-vivo o*ptimization study was also designed to observe the MTD and PK of 1:4 and 1:20 ND in mice. The MTD study indicated that out of several doses tested in the male and female BALB/c mice, the highest dose was well tolerated without any adverse clinical observation. This observation was made based on the visible symptoms as observed by the researcher. PK analysis was performed on the measurable plasma concentration of TFV after administration in two different iv formulations, an ND formulation, and FD-TFV. The terminal $t_{1/2}$ was similar for both the ND formulation and FD-TFV and ranged from 4.9 - 5.3 hours. In male mice, the pharmacokinetic parameters varied slightly between the two formulations, with AUC values about 10% higher using the FD-TFV group. Females treated with FD-TFV exhibited the highest group AUC values with a group AUC values about 2-fold higher than the ND formulation. This group also had lower Cl and Vz values compared to females treated with the ND formulation.

In comparison, administration of unformulated FD-TFV to female mice resulted in parameters consistent with plasma exposure that was 2-fold higher (C_0, AUC_{last}, and AUC_{inf})

while Cl and Vz were lower using sterile saline compared with the ND formulation. This may have been attributed to individual animal variation as one female mouse was found to have higher plasma concentrations at the first timepoint than the others in the group. The observation indicated that the ND formulation has very similar properties to the FD-TFV. Overall, there were no significant difference in TFV pharmacokinetics when administered in an ND formulation than the FD-TFV. Therefore, there was a need to improve the formulation structure before it is considered significantly advantageous over unformulated TFV in clinical settings.

Both *in-vitro* and *in-vivo* characterization studies indicate further optimization of the formulation to obtain a more significant PK. Therefore, the structural lipid composition of the ND was changed to some extent to more closely aligned with a liposomal structure. The change in structure has provided more stability in holding TFV within its aqueous core and indicates extended drug release properties within our study and has been well documented to have sustained release properties because of their amphiphilic nature [89]. Liposomes are capable of holding a larger drug holding capacity and increase in sustained release capacity. The drug release study has shown more retention of TFV compared to FD-TFV, which is significant. We did observe a downward trend in FD-TFV after 4 days of the dissolution study which was different from was observed in from our NDs FD-TFV, despite similar set up. Cause for the downward trend may due to a breakdown of TFV in the release medium due to several factors, particularly under hydrolytic conditions as TFV has been previously found to exhibit degradation under acidic and alkaline conditions [90]. In our dissolution study, pH was not considered, but we will consider pH and repeat experiment to confirm free drug kinetics in future studies. However, it is notable to note that encapsulation of TFV within the liposome can protect TFV from degradation, even in the hydrolytic conditions seen in this dissolution study.

An MTS and ROS assay were not necessary in this formulation as they have been previously characterized by the similar bicellar formulation that retains the same chemical composition [31]. Moreover, the liposome formulation has been previously well-documented to have a non-toxic nature, be biocompatible, versatile and have the ability to carry diverse chemical payloads [35, 89]. Structurally, liposomes are one of the most versatile and sophisticated nanoparticle types as they have the capacity to deliver several biologically active compounds and macromolecules such as DNA, peptides, proteins and imaging agents both in the lipid bilayer and lumen [91]. While this study did not observe the TFV encapsulated liposome's release through the BBB *in-vitro*, a previous studies have observed the successful delivery of a liposome drug carrier across the BBB *in-vitro* and *in-vivo* and we can expect liposomes to pass the BBB as efficiently as NDs [92, 93].

Overall, the study established that ND could provide drug stability and sustained drug release properties to the TFV formulation. However, liposomal formulations have provided a promising alternative to deliver drug, further characterized in *in-vivo* study. This is the first time ND formulation was characterized for antiretroviral drug delivery to the brain and its potential for anti-HIV treatment.

CHAPTER V

CONCLUSION

In this master thesis, we hypothesized that a nanodisc-based delivery of TFV would be safe and effectively perform extended -release, which will help in HIV-1 treatment to the brain. While ND offers an attractive solution for the treatment of HIV-1 latent reservoirs within the brain, we observed that various factors could hinder ND's potentials to become a successful formulation for *in-vivo* study and clinical trial. An increase in the ND's lipid content, seen in the 1:20 formulation, could affect the cellular environment when using higher concentrations. However, the more lipid content within the 1:20 formulation allows it to have a more stable formulation than the 1:4 formulation, enabling it to have a more sustained drug release for a more extended period. In the meantime, the 1:4 formulation is shown to have minimal cytotoxic on neuronal cells but has a less sustained drug release *in-vitro* and *in-vivo* studies. The liposomal structure has shown a significant improvement in the sustained drug release of TFV. A further *in-vivo* characterization would be needed to confirm this observation further. Overall, this study's results contribute to developing a nanoformulation-based delivery towards the brain to treat HIV-1.

REFERENCES

1. HIV/AIDS, J.U.N.P.o., *Global HIV & AIDS statistics—2020 fact sheet.* UNAIDS. org (http://www.unaids.org/sites/default/files/media_asset/UNAIDS_FactSheet_en.pdf, 2020.

2. Naif, H.M., *Pathogenesis of HIV infection.* Infectious disease reports, 2013. **5**(11): p. 26-30.

3. Cummins, N.W. and A.D. Badley, *Making sense of how HIV kills infected CD4 T cells: implications for HIV cure.* Molecular and Cellular Therapies, 2014. **2**(1): p. 20.

4. Rao, K.S., A. Ghorpade, and V. Labhasetwar, *Targeting anti-HIV drugs to the CNS.* Expert Opinion on Drug Delivery, 2009. **6**(8): p. 771-784.

5. Barré-Sinoussi, F., A.L. Ross, and J.-F. Delfraissy, *Past, present and future: 30 years of HIV research.* Nature Reviews Microbiology, 2013. **11**(12): p. 877-883.

6. B. Nachega, J., et al., *HIV Treatment Adherence, Drug Resistance, Virologic Failure: Evolving Concepts.* Infectious Disorders - Drug Targets, 2011. **11**(2): p. 167-174.

7. Gardner, E.M., et al., *Antiretroviral medication adherence and the development of class-specific antiretroviral resistance.* AIDS (London, England), 2009. **23**(9): p. 1035.

8. Chopra, N.K., H. Ni, and V. Lim, *Past Present and Future Status of HIV-AIDS Pandemic Problem in World.* Microbiol Infect Dis, 2019. **3**(1): p. 1-6.

9. Taylor, B.M., et al., *An alteration of human immunodeficiency virus gp41 leads to reduced CCR5 dependence and CD4 independence.* Journal of virology, 2008. **82**(11): p. 5460-5471.

10. Mamo, T., et al., *Emerging nanotechnology approaches for HIV/AIDS treatment and prevention.* Nanomedicine (Lond), 2010. **5**(2): p. 269-85.

11. Richman, D.D., et al., *The Challenge of Finding a Cure for HIV Infection.* Science, 2009. **323**(5919): p. 1304-1307.

12. Ghosh, A.K., A. Sarkar, and H. Mitsuya, *HIV-Associated Neurocognitive Disorder (HAND) and the Prospect of Brain-Penetrating Protease Inhibitors for Antiretroviral Treatment.* Medical research archives, 2017. **5**(4).

13. Atluri, V.S.R., et al., *Effect of human immunodeficiency virus on blood-brain barrier integrity and function: an update.* Frontiers in Cellular Neuroscience, 2015. **9**.

14. Schwartz, C. and O. ROHR, *Microglial cells: the main HIV-1 reservoir in the brain.* Frontiers in cellular and infection microbiology, 2019. **9**: p. 362.

15. Saraiva, C., et al., *Nanoparticle-mediated brain drug delivery: overcoming blood–brain barrier to treat neurodegenerative diseases.* Journal of Controlled Release, 2016. **235**: p. 34-47.

16. Sagar, V., et al., *Towards nanomedicines for neuroAIDS.* Reviews in Medical Virology, 2014. **24**(2): p. 103-124.

17. Joseph, S.B., et al., *HIV-1 target cells in the CNS.* Journal of NeuroVirology, 2015. **21**(3): p. 276-289.

18. Louboutin, J.-P., et al., *HIV-1 gp120-Induced Injury to the Blood-Brain Barrier: Role of Metalloproteinases 2 and 9 and Relationship to Oxidative Stress.* Journal of Neuropathology & Experimental Neurology, 2010. **69**(8): p. 801-816.

19. Asahchop, E.L., et al., *Reduced antiretroviral drug efficacy and concentration in HIV-infected microglia contributes to viral persistence in brain.* Retrovirology, 2017. **14**(1).

20. Patra, J.K., et al., *Nano based drug delivery systems: recent developments and future prospects.* Journal of Nanobiotechnology, 2018. **16**(1).

21. Arca, H.Ç., et al., *Multidrug, Anti-HIV Amorphous Solid Dispersions: Nature and Mechanisms of Impacts of Drugs on Each Other's Solution Concentrations.* Molecular Pharmaceutics, 2017. **14**(11): p. 3617-3627.

22. Gerson, T., et al., *Nano-NRTIs demonstrate low neurotoxicity and high antiviral activity against HIV infection in the brain.* Nanomedicine: Nanotechnology, Biology and Medicine, 2014. **10**(1): p. 177-185.

23. Wang, Y., et al., *Delivery of oligonucleotides with lipid nanoparticles.* Advanced drug delivery reviews, 2015. **87**: p. 68-80.

24. Torchilin, V.P., *Recent advances with liposomes as pharmaceutical carriers.* Nature reviews Drug discovery, 2005. **4**(2): p. 145-160.

25. Dreher, M.R., et al., *Tumor vascular permeability, accumulation, and penetration of macromolecular drug carriers.* Journal of the National Cancer Institute, 2006. **98**(5): p. 335-344.

26. Hsu, H.J., et al., *Dendrimer-based nanocarriers: a versatile platform for drug delivery.* Wiley Interdisciplinary Reviews: Nanomedicine and Nanobiotechnology, 2017. **9**(1).

27. Lai, S.-M., et al., *Enhanced Nuclear Localization of Photosensitizer Using Artificial Oil Bodies for Photodynamic Therapy.* Smart Science, 2016. **4**(4): p. 167-172.

28. Patri, A.K., I.J. Majoros, and J.R. Baker, *Dendritic polymer macromolecular carriers for drug delivery.* Current opinion in chemical biology, 2002. **6**(4): p. 466-471.

29. Ashley, C.E., et al., *The targeted delivery of multicomponent cargos to cancer cells by nanoporous particle-supported lipid bilayers.* Nature materials, 2011. **10**(5): p. 389.

30. Liu, M., et al., *The preparation and characterization of micelles from poly (γ-glutamic acid)-graft-poly (L-lactide) and the cellular uptake thereof.* Journal of Materials Science: Materials in Medicine, 2015. **26**(5): p. 1-9.

31. Tahmasbi Rad, A., et al., *Combinational Effects of Active Targeting, Shape, and Enhanced Permeability and Retention for Cancer Theranostic Nanocarriers.* ACS applied materials & interfaces, 2019.

32. Midde, N.M. and S. Kumar, *Development of NanoART for HIV treatment: minding the cytochrome P450 (CYP) enzymes.* Journal of personalized nanomedicine, 2015. **1**(1): p. 24.

33. Gajbhiye, V., et al., *Synthesis, characterization and targeting potential of zidovudine loaded sialic acid conjugated-mannosylated poly(propyleneimine) dendrimers.* European Journal of Pharmaceutical Sciences, 2013. **48**(4-5): p. 668-679.

34. Xing, H., K. Hwang, and Y. Lu, *Recent developments of liposomes as nanocarriers for theranostic applications.* Theranostics, 2016. **6**(9): p. 1336.

35. Sharma, A., S.V. Madhunapantula, and G.P. Robertson, *Toxicological considerations when creating nanoparticle-based drugs and drug delivery systems.* Expert Opinion on Drug Metabolism & Toxicology, 2012. **8**(1): p. 47-69.

36. Liu, Y., et al., *The effects of temperature, salinity, concentration and PEGylated lipid on the spontaneous nanostructures of bicellar mixtures.* Biochimica et Biophysica Acta (BBA)-Biomembranes, 2014. **1838**(7): p. 1871-1880.

37. Iqbal, U., et al., *Small unilamellar vesicles: a platform technology for molecular imaging of brain tumors.* Nanotechnology, 2011. **22**(19): p. 195102.

38. Nieh, M.P., N. Kucerka, and J. Katsaras, *Spontaneously formed unilamellar vesicles.* Methods Enzymol., 2009. **465**: p. 3-20.

39. Ernsting, M.J., et al., *Factors controlling the pharmacokinetics, biodistribution and intratumoral penetration of nanoparticles.* J Control Release, 2013. **172**(3): p. 782-94.

40. Kong, G., R.D. Braun, and M.W. Dewhirst, *Hyperthermia enables tumor-specific nanoparticle delivery: effect of particle size.* Cancer Res, 2000. **60**(16): p. 4440-5.

41. Tan, J., et al., *The influence of size, shape and vessel geometry on nanoparticle distribution.* Microfluid Nanofluidics, 2013. **14**(1-2): p. 77-87.

42. Zhao, N., et al., *Microglia-targeting nanotherapeutics for neurodegenerative diseases.* APL Bioengineering, 2020. **4**(3): p. 030902.

43. Hutter, E., et al., *Microglial Response to Gold Nanoparticles.* ACS Nano, 2010. **4**(5): p. 2595-2606.

44. Aresh, W., et al., *The Morphology of Self-Assembled Lipid-Based Nanoparticles Affects Their Uptake by Cancer Cells.* Journal of Biomedical Nanotechnology, 2016. **12**(10): p. 1852-1863.

45. WHO, *Update of recommendations on first-and second-line antiretroviral regimens.* 2019.

46. Anthonypillai, C., J. Gibbs, and S. Thomas, Cerebrospinal Fluid Research, 2006. **3**(1): p. 1.

47. Fardis, M. and R. Oliyai, *Case Study: Tenofovir Disoproxil Fumarate: An Oral Prodrug of Tenofovir*. Springer New York. p. 1347-1357.

48. Organization, W.H., *World Health Organization model list of essential medicines: 21st list 2019*. 2019, World Health Organization.

49. Pau, A.K. and J.M. George, *Antiretroviral Therapy.* Infectious Disease Clinics of North America, 2014. **28**(3): p. 371-402.

50. Liu, Y., et al., *Stable Discoidal Bicelles: A Platform of Lipid Nanocarriers for Cellular Delivery.* Liposomes: Methods and Protocols, 2017: p. 273-282.

51. Nieh, M.P., et al., *Formation of kinetically trapped nanoscopic unilamellar vesicles from metastable nanodiscs.* Langmuir, 2011. **27**(23): p. 14308-16.

52. Nieh, M.P., et al., *Spontaneously formed unilamellar vesicles with path-dependent size distribution.* Langmuir, 2005. **21**(15): p. 6656-61.

53. Laad, P., et al., *Differential surface properties of commercial crystalline telmisartan samples.* European Journal of Pharmaceutical Sciences, 2013. **49**(2): p. 109-116.

54. Testa, B., et al., *Lipophilicity in molecular modeling.* Pharmaceutical research, 1996. **13**(3): p. 335-343.

55. *Molecular surface lipophilicity potential calculator of Molinspiration Property Calculation Service.* Molecular surface lipophilicity potential calculator of Molinspiration Property Calculation Service. **www.molinspiration.com**

56. DiFabio, J., et al. *The life science x-ray scattering beamline at NSLS-II*. in *AIP Conference Proceedings*. 2016. AIP Publishing.

57. Yang, L., *Using an in-vacuum CCD detector for simultaneous small-and wide-angle scattering at beamline X9.* Journal of synchrotron radiation, 2013. **20**(2): p. 211-218.

58. Roy, U., et al., *Characterization of Nanodiamond-based anti-HIV drug Delivery to the Brain.* Sci Rep, 2018. **8**(1): p. 1603.

59. Roy, U., et al., *The potential of HIV-1 nanotherapeutics: from in vitro studies to clinical trials.* Nanomedicine, 2015. **10**(24): p. 3597-3609.

60. Roy, U., et al., *Specific increase in MDR1 mediated drug-efflux in human brain endothelial cells following co-exposure to HIV-1 and saquinavir.* PloS one, 2013. **8**(10).

61. Gendelman, H., et al., *Comparative manufacture and cell-based delivery of antiretroviral nanoformulations.* International Journal of Nanomedicine, 2011: p. 3393.

62. Nowacek, A.S., et al., *NanoART synthesis, characterization, uptake, release and toxicology for human monocyte–macrophage drug delivery.* Nanomedicine, 2009. **4**(8): p. 903-917.

63. Chen, X., et al., *Model Linking Plasma and Intracellular Tenofovir/Emtricitabine with Deoxynucleoside Triphosphates.* PLOS ONE, 2016. **11**(11): p. e0165505.

64. Liu, Y., et al., *Stable discoidal bicelles: A platform of lipid nanocarriers for cellular delivery*, in *Liposomes*. 2017, Springer. p. 273-282.

65. Adults, P.o.A.G.f. and Adolescents, *Guidelines for the use of antiretroviral agents in adults and adolescents living with HIV*. 2019, Department of Health and Human Services.

66. Organization, W.H., *Consolidated guidelines on the use of antiretroviral drugs for treating and preventing HIV infection: recommendations for a public health approach*. 2016: World Health Organization.

67. Bozzuto, G. and A. Molinari, *Liposomes as nanomedical devices.* International Journal of Nanomedicine, 2015: p. 975.

68. Zhang, W., J. Sun, and Z. He, *The application of open disk-like structures as model membrane and drug carriers.* Asian Journal of Pharmaceutical Sciences, 2013. **8**(3): p. 143-150.

69. Shrestha, H., R. Bala, and S. Arora, *Lipid-based drug delivery systems.* Journal of pharmaceutics, 2014. **2014**.

70. Bahadar, H., et al., *Toxicity of nanoparticles and an overview of current experimental models.* Iranian biomedical journal, 2016. **20**(1): p. 1.

71. Grabowski, N., et al., *Surface coating mediates the toxicity of polymeric nanoparticles towards human-like macrophages.* International Journal of Pharmaceutics, 2015. **482**(1-2): p. 75-83.

72. Lacagnina, M.J., P.D. Rivera, and S.D. Bilbo, *Glial and Neuroimmune Mechanisms as Critical Modulators of Drug Use and Abuse.* Neuropsychopharmacology, 2017. **42**(1): p. 156-177.

73. Wang, *Selective neuronal vulnerability to oxidative stress in the brain.* Frontiers in Aging Neuroscience, 2010.

74. Fu, P.P., et al., *Mechanisms of nanotoxicity: Generation of reactive oxygen species.* Journal of Food and Drug Analysis, 2014. **22**(1): p. 64-75.

75. Manke, A., L. Wang, and Y. Rojanasakul, *Mechanisms of nanoparticle-induced oxidative stress and toxicity.* BioMed research international, 2013. **2013**.

76. Lu, X.-Y., et al., *Polymer nanoparticles.* Progress in molecular biology and translational science, 2011. **104**: p. 299-323.

77. Loftsson, T., *Principles of Drug Degradation*. 2014, Elsevier. p. 5-62.

78. Golla, V.M., et al., *Stability behaviour of antiretroviral drugs and their combinations. 4: Characterization of degradation products of tenofovir alafenamide fumarate and comparison of its degradation and stability behaviour with tenofovir disoproxil fumarate.* Journal of Pharmaceutical and Biomedical Analysis, 2016. **131**: p. 146-155.

79. Li, L., et al., *Performance and Stability of Tenofovir Alafenamide Formulations within Subcutaneous Biodegradable Implants for HIV Pre-Exposure Prophylaxis (PrEP).* Pharmaceutics, 2020. **12**(11): p. 1057.

80. Roy, U., et al., *Preparation and characterization of anti-HIV nanodrug targeted to microfold cell of gut-associated lymphoid tissue.* International Journal of Nanomedicine, 2015: p. 5819.

81. Hua, S., *Comparison of in vitro dialysis release methods of loperamide-encapsulated liposomal gel for topical drug delivery.* International Journal of Nanomedicine, 2014: p. 735.

82. Chauhan, I., et al., *Nanostructured Lipid Carriers: A Groundbreaking Approach for Transdermal Drug Delivery.* Advanced Pharmaceutical Bulletin, 2020. **10**(2): p. 150-165.

83. Bagchi, S., et al., * In-vitro blood-brain barrier models for drug screening and permeation studies: an overview *. Drug Design, Development and Therapy, 2019. **Volume 13**: p. 3591-3605.

84. Best, B.M., et al., *Low Cerebrospinal Fluid Concentrations of the Nucleotide HIV Reverse Transcriptase Inhibitor, Tenofovir.* JAIDS Journal of Acquired Immune Deficiency Syndromes, 2012. **59**(4): p. 376-381.

85. Zhang, F., et al., *Targeting specific cells in the brain with nanomedicines for CNS therapies.* Journal of Controlled Release, 2016. **240**: p. 212-226.

86. Grabrucker, A.M., et al., *Nanoparticle transport across the blood brain barrier.* Tissue Barriers, 2016. **4**(1): p. e1153568.

87. Foroozandeh, P. and A.A. Aziz, *Insight into Cellular Uptake and Intracellular Trafficking of Nanoparticles.* Nanoscale Research Letters, 2018. **13**(1).

88. Wu, M., et al., *Size-dependent cellular uptake and localization profiles of silver nanoparticles.* International journal of nanomedicine, 2019. **14**: p. 4247.

89. Karumanchi, D.K., et al., *Rational design of liposomes for sustained release drug delivery of bevacizumab to treat ocular angiogenesis.* Journal of Drug Delivery Science and Technology, 2018. **47**: p. 275-282.

90. Agrahari, V., et al., *Evaluation of degradation kinetics and physicochemical stability of tenofovir.* Drug Testing and Analysis, 2015. **7**(3): p. 207-213.

91. Vahed, S.Z., et al., *Liposome-based drug co-delivery systems in cancer cells.* Materials Science and Engineering: C, 2017. **71**: p. 1327-1341.

92. Tian, W., et al., *Enhanced efficacy of functionalized epirubicin liposomes in treating brain glioma-bearing rats.* European Journal of Pharmaceutical Sciences, 2010. **41**(2): p. 232-243.

93. Shaw, T.K., et al., *Successful delivery of docetaxel to rat brain using experimentally developed nanoliposome: a treatment strategy for brain tumor.* Drug Delivery, 2017. **24**(1): p. 346-357.

BIOGRAPHICAL SKETCH

Caroline Rose Garcia was born in Brownsville, TX. She earned her high school diploma from Veterans Memorial Early College High School at Brownsville, TX, in June 2016. Shortly after, she was accepted and attended the University of North Texas in Denton, TX. During her undergraduate career, Caroline worked in various research labs both as a student and as an undergraduate research assistant and found a love for research and the sciences. She worked diligently in her studies and completed a Bachelor of Arts in Biology with a minor in Chemistry in Spring 2019. Afterward, in Fall 2019, Caroline was admitted into the graduate program at the University of Texas at Rio Grande Valley in Brownsville, TX, and started working towards completing her graduate education. As a graduate student, Caroline worked as a graduate research assistant and teaching assistant for an undergraduate lab. She was awarded her Master of Science in Biochemistry and Molecular Biology in May 2021. She is available for contact at caro.rgarcia02@gmail.com.